2005

# Edge Detection of Noisy Images Using 2-D Discrete Wavelet Transform

Venkata Ravikiran Chaganti

**THE FLORIDA STATE UNIVERSITY**

**FAMU-FSU COLLEGE OF ENGINEERING**

# EDGE DETECTION OF NOISY IMAGES USING 2-D DISCRETE WAVELET TRANSFORM

**BY**

**VENKATA RAVIKIRAN CHAGANTI**

**A thesis submitted to the**
**Department of Electrical Engineering**
**in partial fulfillment of the**
**requirements for the degree of**
**Master of Science**

**Degree Awarded:**
**Spring Semester, 2005**

The members of the committee approve the thesis of Venkata R. Chaganti defended on April 11th, 2005.

_____

Simon Y. Foo
Professor Directing Thesis

_____

Anke Meyer-Baese
Committee Member

_____

Rodney Roberts
Committee Member

Approved:

_____

Leonard J. Tung, Chair, Department of Electrical and Computer Engineering

_____

Ching-Jen Chen, Dean, FAMU-FSU College of Engineering

The office of Graduate Studies has verified and approved the above named committee members.

*Dedicate to*

*My Father late Dr.Rama Rao, Mother, Brother and Sister-in-law*
*without whom this would never have been possible*

## ACKNOWLEDGEMENTS

I thank my thesis advisor, Dr.Simon Foo, for his help, advice and guidance during my M.S and my thesis. I also thank Dr.Anke Meyer-Baese and Dr. Rodney Roberts for serving on my thesis committee. I would like to thank my family for their constant support and encouragement during the course of my studies.

I would like to acknowledge support from the Department of Electrical Engineering, FAMU-FSU College of Engineering. A special thanks goes to Electrical Engineering Graduate student Jason Isaacs for all the encouragement and help in the laboratory. I would like to thank all my friends in the laboratory.

## TABLE OF CONTENTS

## LIST OF FIGURES

# CHAPTER 1

# INTRODUCTION

## 1.1 INTRODUCTION TO EDGE DETECTION

Points in an image where brightness changes abruptly are called edges or edge points. There are different types of sharp changing points in an image. Edges can be created by shadows, texture, geometry, and so forth. Edges can also be defined as discontinuities in the image intensity due to changes in image structure. These discontinuities originate from different features in an image. Edge points are to be associated with the boundaries of objects and other kinds of changes. Edges within an image generally occur at various resolutions or scales and represent transitions of different degree, or gradient levels.

Edge detection refers to the process of identifying and locating sharp discontinuities in an image. There are many ways to perform edge detection. However, most of them may be grouped into two categories, namely, gradient based edge detection and Laplacian-based edge detection. In the gradient based edge detection, we calculate an estimate of the gradient magnitude using the smoothing filter and use the calculated estimate to determine the position of the edges. In other words the gradient method detects the edges by looking for the maximum and minimum in the first derivative of the image. In the Laplacian method we calculate the second derivative of the signal and the derivative magnitude is maximum when second derivative is zero. In short, Laplacian method searches for zero crossings in the second derivative of the image to find edges.

An edge map detected from tits original image contains major information, which only needs a relatively small amount of memory space to store. The original image can be easily restored from its edge map. Various edge detection algorithms have been developed in the process of finding the perfect edge detector. Some of the edge detection operators that are discussed in this thesis are Robert, Prewitt, Sobel, FreiChen and Laplacian Of Gaussian (LOG) operators. Prewitt, Sobel and FreiChen are 3x3 masks operators. The Prewitt masks are simpler to implement than the Sobel masks, but the later have slightly superior noise suppression characteristics. LOG is a more complicated edge detector than the previous mentioned operators.

## 1.2 EFFECTS OF NOISE ON EDGE DETECTION

Edge detection is susceptible to noise. This is due to the fact that the edge detectors algorithms are designed to respond to sharp changes, which can be caused by noisy pixels. Noise may occur in digital images for a number of reasons. The most commonly studied noises are white noise, “salt & pepper” noise and speckle noise. The effect of noise on edge detection is shown in figure 1.1.

To reduce the effects of noise, preprocessing of the image is performed. The preprocessing can be performed in two ways, filtering the image with a Gaussian function, or by using a smoothing function. The problem with the above approaches is that the optimal result may not be obtained by using a fixed operator.

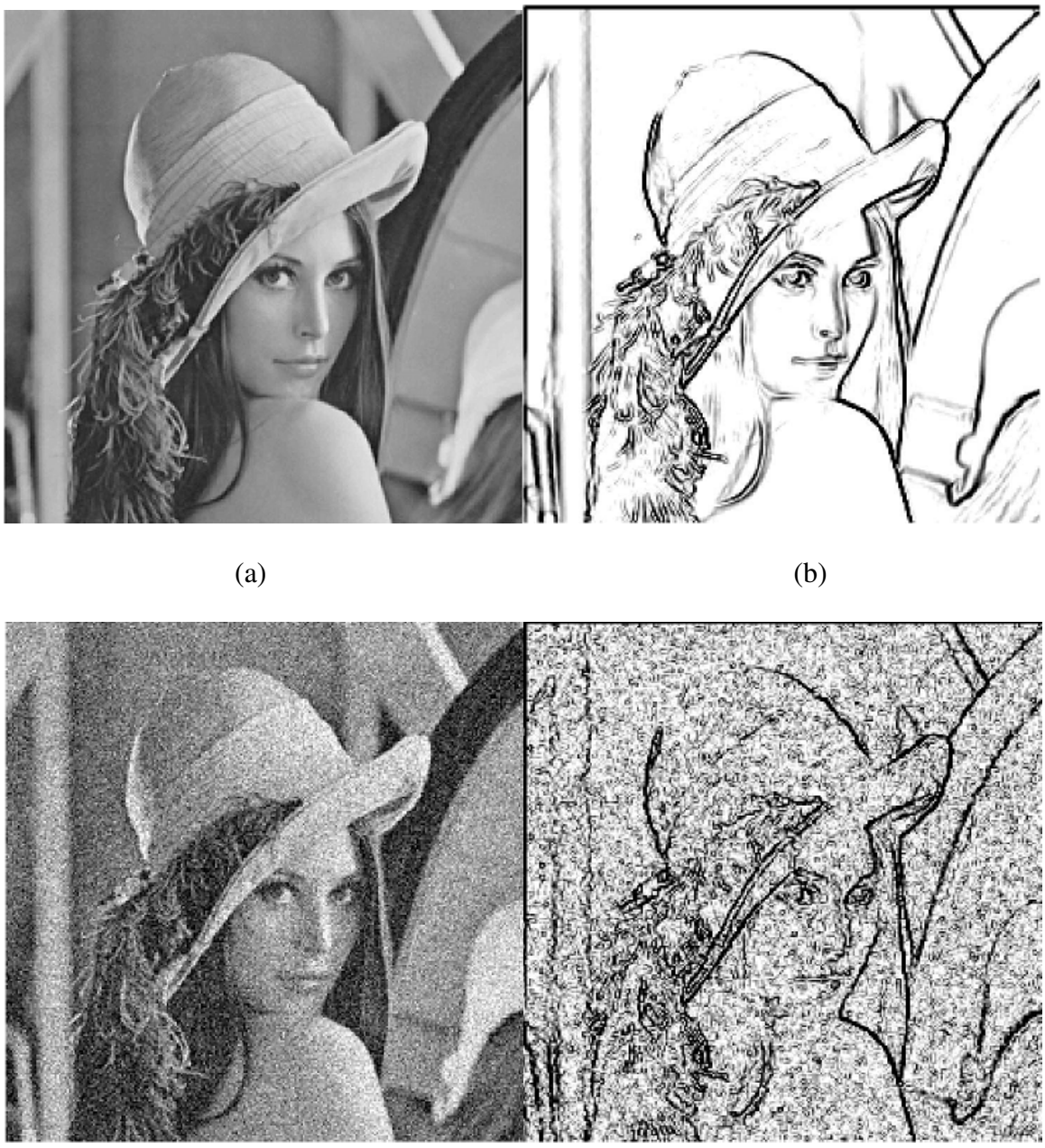

(a) (b)

(c) (d)

Figure 1.1: (a) the image of “lenna” without noise, (b) the edge detection without noise. (c) “lenna” image with noise (d) the edge detection with noise.

.

## 1.3 ADVANTAGES OF WAVELETS OVER FOURIER TRANSFORM

Most of the signals in practice are time-domain signals. When we plot time-domain signals, we obtain a time-amplitude representation of the signal. In many cases, the most important information is hidden in the frequency content of the signal. The frequency spectrum of a signal shows what frequencies exist in the signal.

Fourier transform (FT) and inverse Fourier transform are defined as

$$X(f) = \int_{-\infty}^{\infty} x(t) e^{-j2\pi ft} dt \qquad x(t) = \int_{-\infty}^{\infty} X(f) e^{j2\pi ft} df \tag{1.1}$$

Fourier transform gives the frequency information of the signal, but it does not tell us when in time these frequency components exist. The information provided by the integral corresponds to all time instances because the integration is done for all time intervals. It means that no matter where in time the frequency *f* appears, it will affect the result of the integration equally. This is why Fourier transform is not suitable for non-stationary signals.

To overcome this weakness, short time Fourier transform (STFT) was developed. In STFT the signal is divided into small segments which can be assumed to be stationary. In STFT of the signal multiplied by a window function within the Fourier integral. If the window length is infinite, it becomes the Fourier transform. In order to obtain the stationary signal, the window length must be short enough. The narrower windows affords better time resolution and a better stationary signal, but at the cost of poorer frequency resolution. One problem with STFT is that one cannot know what spectral components exist at what points of time. One can only know the time intervals in which certain band of frequencies exist.

The wavelet transform evolved as an alternative approach to STFT to overcome the resolution problem. The wavelet transform is similar to the STFT in that the signal is multiplied by a function similar to windows function in STFT, but the transform is done separately for different segments of the signal. The main difference between the STFT and the wavelet transform is that in wavelet transform, the width of the window is changed as the transform is computed for every single spectral component.

## 1.4 EVOLUTION OF WAVELETS

Wavelets represent a departure from Fourier analysis. Actually wavelet analysis is a natural extension to Fourier analysis through its mathematical relationship dated all the way back to the work of Joseph Fourier in the nineteenth century. Fourier laid the foundation for the frequency analysis, which proved to be enormously important.

Fourier asserted that any $2\pi$ -periodic function *f(x)* is the sum of its Fourier series.

$$a_0 + \sum_{k=1}^{\infty} (a_k \cos kx + b_k \sin kx) \tag{1.2}$$

The coefficients $a_0, a_k$ and $b_k$ are calculated by

$$a_0 = \frac{1}{2\pi}\int_0^{2\pi} f(x)dx\,,\ a_k = \frac{1}{\pi}\int_0^{2\pi} f(x)\cos(kx)dx\,, b_k = \frac{1}{\pi}\int_0^{2\pi} f(x)\sin(kx)dx \tag{1.3}$$

Mathematicians gradually turned their attention from frequency-based analysis to scale-based analysis due to the fact that measuring average fluctuations at different scales might prove less sensitive to noise.

The first mention of wavelets appeared in an appendix to the thesis of A. Haar (1909). One property of the Haar wavelet is that it has compact support, which means that it vanishes outside of a finite interval. Unfortunately, Haar wavelets are not continuously differentiable which somewhat limits their applications.
By using a scale-varying basis function called the Haar basis function, Paul Levy, a 1930s physicist, investigated Brownian motion, a type of random signal. He found the Haar basis function superior to the Fourier basis functions for studying small complicated details in the Brownian motion.

Another 1930s research effort by Littlewood, Paley, and Stein [43] involved computing the energy of a function *f(x)*:

$$energy = \frac{1}{2}\int_{0}^{2\pi} \left| f(x) \right|^2 dx \tag{1.4}$$

The computation produced different results if the energy was concentrated around a few points or distributed over a larger interval. Their work provided David Marr [44] with an effective algorithm for numerical image processing using wavelets in the early 1980s.

Between 1960 and 1980, the mathematicians Guido Weiss and Ronald R. Coifman [45] studied the simplest elements of a function space, called atoms, with the goal of finding the atoms for a common function and finding the "assembly rules" that allow the reconstruction of all the elements of the function space using these atoms. In 1980, Grossman and Morlet [47], broadly defined wavelets in the context of quantum physics.

In 1985, Stephane Mallat gave wavelets an additional jump-start through his work in digital signal processing. He discovered some relationships between quadrature mirror filters, pyramid algorithms, and orthonormal wavelet bases. Inspired by Mallat's work, Yves Meyer[48] constructed the first non-trivial wavelets. Unlike the Haar wavelets, the

Meyer wavelets are continuously differentiable. A couple of years later, Ingrid Daubechies used Mallat's work to construct a set of wavelet orthonormal basis functions that are perhaps the most elegant, and have become the cornerstone of wavelet applications today.

Stephane Mallat [17, 19] made a decisive step in the theory of wavelets in 1987 when he proposed a fast algorithm for the computation of wavelet coefficients. He proposed pyramidal schemes that decompose signals into subbands. These techniques can be traced back to the 1970's when there techniques were used to reduce quantization noise. The framework that unifies these algorithms and the theory of wavelets is the concept of a multi-resolution analysis (MRA). MRA is similar to subband decomposition and coding, where for coding efficiency, the signal is divided into a set of frequency bands. In 1997, Chui and Wang [49] further discussed the asymptotically optimal time frequency localization by scaling functions and wavelets.

## 1.5 EDGE DETECTION USING WAVELETS: SOME BACKGROUND

Edge detection is a common operation issue in image analysis. Edges can be considered as transients in a signal or mathematically defined as local singularities. The Fourier transform is global and not well adapted to local singularities.

Canny [51] proposed the operators of different widths to obtain better signal to noise ratios in the detection of patterns that appear at different scales in the image. Marr [44] proposed a multiresolution scheme to detect primitives related to human visual system behavior. Bergholm [50] used Canny's operator and was able to differentiate between shadow contours from perfect ones. All of them used multiresolution scheme but had difficulty in analyzing the information appearing at different scales. After the introduction of wavelet multiresolution analysis that was based on the Gaussian kernel, the results obtained for edge detection and classification of the edges appearing in the image were better.

Wavelet analysis is a local analysis and is suitable for time-frequency analysis. In wavelet edge detection technique, the transform used is Discrete Wavelet Transform (DWT) and the filter is one which searches for the local maxima in a wavelet domain. The wavelet transform offers a multiscale analysis, which can be applied to edge detection.

Mallat and Zhong [17, 19] utilized the local maxima of the absolute value of the wavelet transform to do edge detection. Peytavin studied a multi-oriented and multi-resolution edge detection technique using a wavelet, which is the first derivative of the smoothing function. Barlaud used a biorthogonal wavelet transform for edge detection.

## 1.6 OVERVIEW OF THE THESIS

The purpose of this thesis is to find an optimum wavelet or cascade of wavelets for edge detection. This thesis also deals with the effects of noise on images and the edge detection of noisy image both by tradition edge detectors and wavelet edge detectors.

Chapter 2 introduces the concepts of Continuous wavelet transforms and multiresolution analysis (MRA). The scale of a wavelet function is defined. The approximation of Gaussian filter with B-spline is discussed. The role of number of vanishing moments in a given wavelet is also discussed.

Chapter 3 deals with the different types of classical edge detection techniques and various edge detectors are discussed in depth regarding the working and implementation.

Chapter 4 discusses the analysis of different wavelet families for edge detection. It also brings out the superiority of wavelet edge detection over traditional operators.

Finally, Chapter 5 shows the development of multiscale wavelet edge detection and the results of different images being applied to edge detection techniques. It also discusses the optimization of the best suitable wavelet for edge detection. Lastly, it presents some future research topics.

# CHAPTER 2

# INTRODUCTION OF WAVELET TRANSFORM

## 2.1 INTRODUCTION

One of the major disadvantages of the Fourier transform is the lack of localization in what the Fourier transform considers phenomena in an infinite interval. Basically, it decomposes a signal in plane waves, which oscillates infinitely with the same period and these waves do not have local characteristics. Another major flaw in the Fourier analysis is the separate description and representation of time and frequency.

The wavelet transform is quite similar to the Short Time Fourier Transform (STFT) except the window is not fixed as in STFT. The wavelet transform is more flexible and it can be any chosen function, can be shifted and dilated to analyze signals. Wavelets can be interpreted as small waves abstractly expressed in a zero mean value. The wavelet transform map a time function into a two dimensional function of $a$ and $b$. The parameter $a$ is called the scale and it scales a function by compressing or stretching it. The parameter $b$ is called the translation of the wavelet function along the time axis.

A wavelet function $\psi(t)$ , can be written as

$$\psi_a(t-b) = \frac{1}{\sqrt{|a|}}\psi(\frac{t-b}{a}) \qquad (2.1)$$

where $a$ is the scaling factor, $b$ the translation along the axis and $\frac{1}{\sqrt{|a|}}$ is a normalized factor.

## 2.2 DIFFERENCES BETWEEN STFT AND WAVELET TRANSFORM

In STFT at an analyzing frequency of $\omega_o$ , changing window width will increase or decrease the number of cycles of $\omega_o$ inside the window. In wavelet transform, since the window width changes mean dilation or compression. The carrier frequency become $\omega_o/a$, for a window width change from T to $a$T as shown in the figure 2.1. In wavelet transform there is center frequency shift accompanied by the window width change unlike the STFT where there is no center frequency shift.

## 2.3 THE CONTINUOUS WAVELET TRANSFORM

In the continuous wavelet transform, a function $\psi$ ("psi") is used to create a family of wavelets $\psi(at+b)$ where $a$ and $b$ are real numbers and the parameter $a$ is dilating the function $\psi$ and $b$ the translating it. Note that the word "continuous" refers to the transform and not the wavelets.

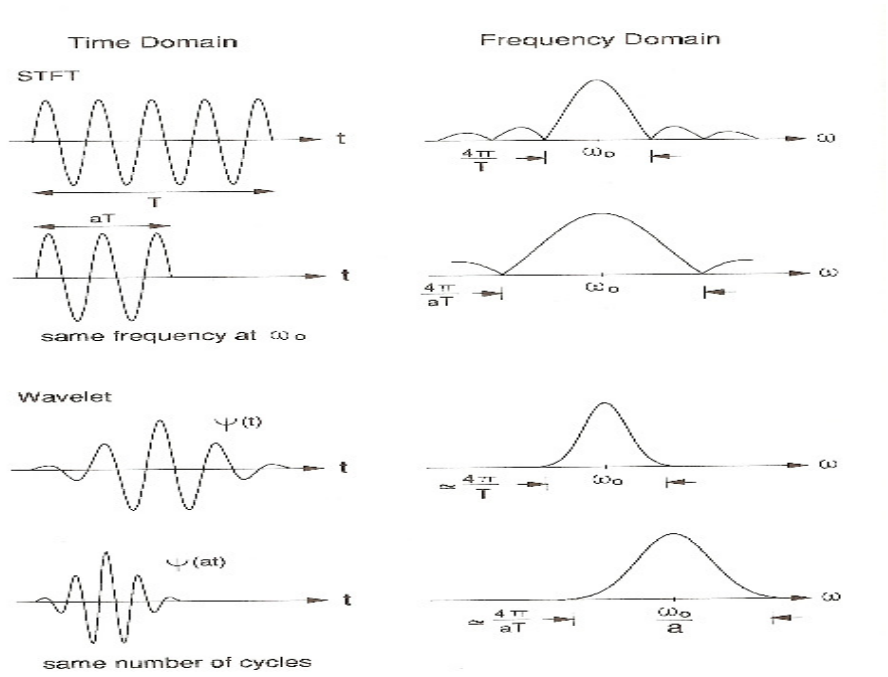


Figure 2.1: Comparison between STFT and wavelet transform

The continuous wavelet transform turns a signal *s(t)* into a function with two variables (scale and time) as shown in equation

$$c(a,b) = \int s(t)\psi(at+b)dt \qquad (2.2)$$

where $\psi$ is the mother wavelet and *c* the coefficients of the wavelet transform

In any image coding application, perfect reconstruction is most important. Even after image processing the reconstructed images will only be an approximation of the original image. If a transform is not invertible it can be said to have dissimilar patterns processing identical transforms.

Lemma 2.1: Let $s(t) \in L^2(R)$ and the CWT of *s(t)*, with respect to a wavelet $\psi(t)$, be

$$CWT(a, b) = \frac{1}{\sqrt{|a|}} \int s(t)\psi(\frac{t-b}{a})dt \qquad (2.3)$$

If the $\psi(t)$ is such that this transform is invertible, then

$$s(t) = \frac{1}{c_\psi} \int_{-\infty}^{\infty} \int_{a>0}^{\infty} CWT(a,b) \frac{1}{\sqrt{a}} \psi(\frac{t-b}{a}) \frac{1}{a^2} dadb \qquad (2.4)$$

where $c_\psi$ is a constant that depends only on $\psi(t)$ and *a* positive. The constant has a value of

$$c_\psi = \int_0^{\infty} \frac{|\psi(\omega)|^2}{\omega} d\omega < \infty \qquad (2.5)$$

which in turn imposes an admissibility condition on $\psi(t)$. For $c_\psi < \infty$, $\psi(t)$ must be such that

$$|\psi(\omega)| < \infty, \text{ for any } \omega \qquad (2.6)$$

and $\psi(0) = 0$, implying that

$$\int \psi(t)dt = 0 \qquad (2.7)$$

meaning that $\psi(t)$ cannot have non-zero dc. The proof of invisibility of the CWT is obtained by applying the resolution of identity theorem.

This theorem state that the transformation of a one dimensional signal *s(t)* into two dimensional wavelet domain of *(a,b)* is invertible if the transformation is an isometry up to a constant factor $c_\psi$ .

## 2.4 MULTIRESOLUTION ANALYSIS (MRA)

Multiresolution analysis is the heart of wavelet analysis. Stephane Mallat linked orthogonal wavelets with the filters used in signal processing with the multiresolution theory. Multiresolution analysis with wavelets provides an important tool to decompose information in a signal into information at separate scales. The wavelet is upstaged by a new function, the scaling function, which gives a series of pictures of the signal, each differing by a factor of two from the previous resolution. In one direction, these successive images approximate the signal with greater and greater precision, approaching the original. In the other direction, they approach zero, containing less and less information.

MRA is the decomposition of a signal *s(t)* into components of different scales of $2^{-m}$, where m is an integer. Associating with each scale is a subspace $V_m$. The subspaces are time functions, which satisfy the following conditions.

1.) The sequence is nested, i.e., for all *j*

$$V_j \subset V_{j+1}$$

$$\{0\} \to \ldots V_2 \subset V_1 \subset V_0 \subset V_{-1} \subset V_{-2} \subset V_{-3} \ldots \to L^2(R)$$

If a function *s(t)* is in $V_j$, then *s(2t)* is in $V_{j-1}$ and vice versa.

2.) Existence of orthonormal scaling function

There exits a scaling function also called as father wavelet, $\phi(t) \in V_0$ such that the set

$$\left\{ \phi_{mn}(t) = 2^{-\frac{m}{2}} \phi(2^{-m}t - n) \right\} : n = integer \qquad (2.8)$$

is an orthonormal basis that spans $V_m$.

The union of the space is dense, i.e. for all f in $L^2(R)$

$$\lim_{j \to +\infty} \left\| f - P_j^0 f \right\|_{L^2} = 0, \qquad (2.9)$$

where $P_j^0$ is the orthonormal projection onto $V_j$

3.) Basis function defined by two-scale difference equations

Since $\phi_{0n}(t)$ spans $V_0$ and $\phi_{-1n}(t)$ spans $V_{-1}$ and $V_{-1}$ contains $V_0$, $\phi_{00}(t) = \phi(t)$ is a linear combination of $\phi_{-1n}(t) = \sqrt{2}\phi(2t - n)$, i.e.,

$$\phi(t) = 2\sum_{l=0}^{p-1} g(l)\phi(2t - l) \qquad (2.10)$$

which is a two-scale difference equation, with *g(l)* the coefficients of combination.

4.) The intersection of the spaces is reduced to the null function. i.e.

$$\lim_{j \to -\infty} \left\| P_j^0 f \right\|_{L^2} = 0, \qquad (2.11)$$

5.) There exists a function $\varphi \in V_0$ such that the family

$$\varphi(. - k), k \in \mathrm{Z},$$

is a Riesz basis of $V_0$.

## 2.5 BUILDING A WAVELET

The 2- scale equation is given by

$$\phi(x) = \sum_k h_k \phi_{1,k}(x) = \sum_k h_k \sqrt{2}\phi(2x-k) \qquad (2.12)$$

where $h_k$ is given by

$$h_k = \langle \phi, \phi_{1,k} \rangle \qquad (2.13)$$

Consider $g(x) \in V_1$ and $g(x) = \sum_k g_k \sqrt{2}\phi(2x-k)$ *(2.14)*

where $g_k = (-1)^k h_{1-k}$

therefore $g(x) = \sum_k (-1)^k h_{1-k} \phi_{1,k}(x)$ *(2.15)*

we define $g_{jk}(x) = 2^{\frac{j}{2}} g(2^j x - k)$ *(2.16)*

so $\langle g_{0k}, \phi_{0l} \rangle = 0$ for all integers k and l

Define $W_0$ to be space spanned by $g_{0k}$, which show $W_0$ is the orthogonal complement of $V_0$ in $V_1$.

$$V_1 = V_0 \oplus W_0$$

Similarly let $W_j$ be spanned by $g_{jk}$, which shows $W_j$ is orthogonal complement of $V_j$ in $V_{j+1}$.

Hence

$$\begin{array}{ccccccc} \ldots & V_0 & \rightarrow & V_1 & \rightarrow & V_2 & \ldots \\ & & \nearrow & & \nearrow & & \\ \ldots & W_0 & & W_1 & & W_2 & \ldots \end{array}$$

Therefore $$V_j = V_0 \oplus W_0 \oplus W_1 \ldots \oplus W_{j-1}$$

Therefore, $g_{jk}$ are orthogonal basis for $L^2(R)$. They are orthonomal also.

Hence proving that $\psi(x) = g(x)$ is a wavelet

The discrete wavelet transform projects *f* onto spaces $V_j$ and $W_j$. It is given as

$$f = proj_{v_{j0}} f + \sum_{i=j0}^{\infty} proj_{W_i} f \qquad (2.17)$$

This relation is called a Quadrature mirror relation, *h* and *g* being the quadrature mirror filters. *h* is a low pass or averaging filter whereas *g* is a high pass or differencing filter. Different filters give different wavelets and different scaling functions $\phi$ give different wavelets $\psi$. Building of other types of wavelets is discussed in detail in the third chapter of this thesis.

## 2.6 WAVELET DECOMPOSITION AND RECONSTRUCTION

Consider $c_{j,k}$ as the wavelet coefficient for $\phi$

$$c_{j,k} = \langle \phi, \phi_{j,k} \rangle = \int \phi(x)\phi_{j,k}(x)dx \qquad (2.18)$$

We can use the above notation for any function *f* that interest us

Therefore $$c_{j,k} = \langle f, \phi_{j,k} \rangle = \int f(x)\phi_{j,k}(x)dx \qquad (2.19)$$

Similarly $$d_{j,k} = \langle f, \psi_{j,k} \rangle = \int f(x)\psi_{j,k}(x)dx \qquad (2.20)$$

Suppose we have high-level coefficients $c_{j,k}$ for a given function *f* we get obtain the lower level coefficients, course and detail coefficients.

$$c_{j-1,k} = \sum_l h_{l-2k} c_{j,l} \qquad (2.21)$$

$$d_{j-1,k} = \sum_l g_{l-2k} c_{j,l} \qquad (2.22)$$

Recalling the MRA structure of spaces consider the coefficient in the same way, thereby the coefficients span out as

$$\ldots\ c_{j-2} \leftarrow\ c_{j-1} \leftarrow\ c_j\ \ldots$$

$$\swarrow \qquad \swarrow$$

$$\ldots\ d_{j-2} \qquad d_{j-1} \qquad \ldots$$

The above process is called downsampling. The downsampled coefficients will be exactly half of the number of the previous coefficients.

We can write

$$\sum_k c_{j,k}\phi_{j,k}(x) = \sum_k c_{j-1,k}\phi_{j-1,k}(x) + \sum_k d_{j-1,k}\psi_{j-1,k}(x) \qquad (2.23)$$

If $f = \phi$, the $d_{j-1,k} = 0$ and if we continue with the MRA chain as above, we can show that

$$\sum_k c_{j,k}\phi_{j,k}(x) = \sum_k c_{j0,k}\phi_{j0,k}(x) + \sum_{j=j0}^{j-1} \sum_k d_{j,k}\psi_{j,k}(x) \qquad (2.24)$$

The above equation is an interpretation of the Discrete Wavelet Transform (DWT).

Wavelet reconstruction is very much similar to the wavelet decomposition. We use the MRA chain model to upsample the coefficients. In reconstruction we consider the lower level coefficients and the detail coefficients and combine them to get the upper level coefficients. Each time we do this addition the number coefficients is double the number of coefficients of the previous low-level coefficients.

## 2.7 DISCRETE WAVELET TRANSFORM

Unlike the Fourier transform, the discrete wavelet transform (DWT) is not a single object. The concept of DWT was first introduced by Stromberg from the Littlewood-Paley decomposition of operators a function. The two dimensional DWT descends from the Laplacian pyramid scheme of Burt and Adelson as shown in figure 2.2.

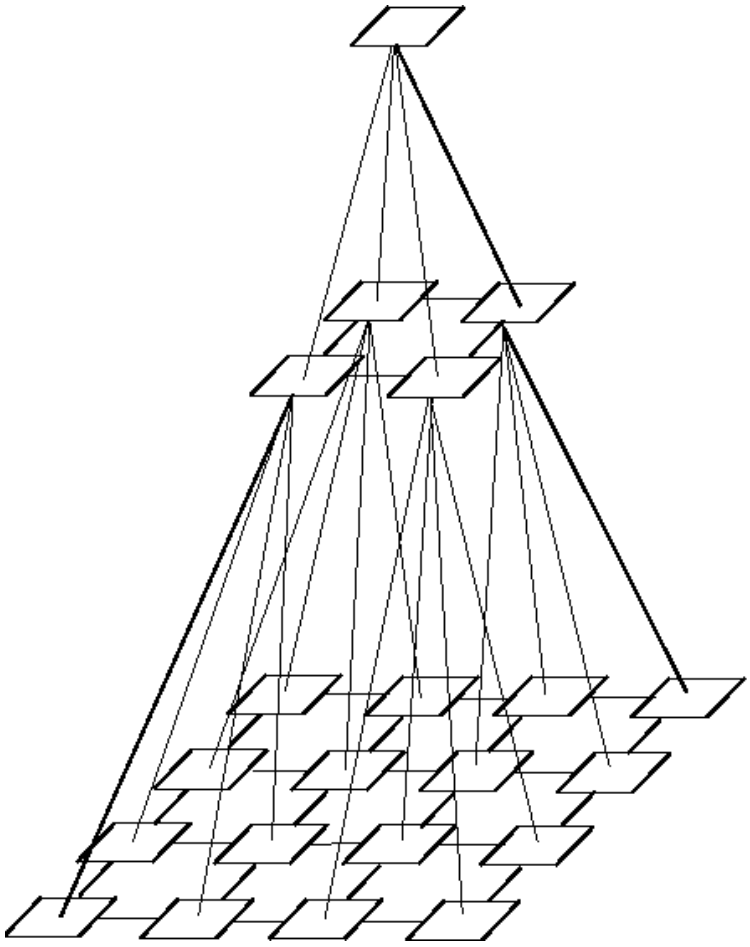

Figure 2.2: Laplacian Pyramid developed by Burt and Adelson

If the function being expanded is a sequence of numbers, like samples of a continuous function *f(x),* the resulting coefficients are called the discrete wavelet

transform (DWT) of *f(x).* DWT transforms a discrete time signal to a discrete wavelet representation.

We do not calculate the DWT in terms of matrices due to the issue of storage, instead we use filters to compute the DWT.

Let $a = \{\ldots,\ a_{-1}, a_0,\ a_1, \ldots\}$ be a sequence. Lets consider two-filter impulses $h$ and $g$.

We define convolutions as

$$(Ha)_k = \sum_l h_{l-2k} a_k \qquad (2.25)$$

$$(Ga)_k = \sum_l g_{l-2k} a_k \qquad (2.26)$$

where H and G corresponds to one step of the DWT (up or down)

In the decomposition, the function is successively convolved with the two filters $H$ (low frequencies) and $G$ (high frequencies). Each resulting function is decimated by suppression of one sample out of two. The high frequency signal is left, and we iterate with the low frequency signal. In the reconstruction, we restore the sampling by inserting a 0 between each sample, then we convolve with the conjugate filters $\tilde{H}$ and $\tilde{G}$, we add the resulting functions and we multiply the result by 2. We iterate up to the smallest scale.

The 2D algorithm is based on separate variables leading to prioritizing of x and directions. The scaling function is defined by

$$\phi(x, y) = \phi(x)\phi(y) \qquad (2.27)$$

The detail signal is obtained from three wavelets:

- a vertical wavelet :

$$\psi^1(x, y) = \phi(x)\psi(y) \tag{2.28}$$

- a horizontal wavelet:

$$\psi^2(x, y) = \psi(x)\phi(y) \tag{2.29}$$

- a diagonal wavelet:

$$\psi^3(x, y) = \psi(x)\psi(y) \tag{2.30}$$

which leads to three sub-images in each of the decomposition levels as shown in the figure 2.3. An example of the decomposition levels using the image of "Lenna" is shown in figure 2.4.

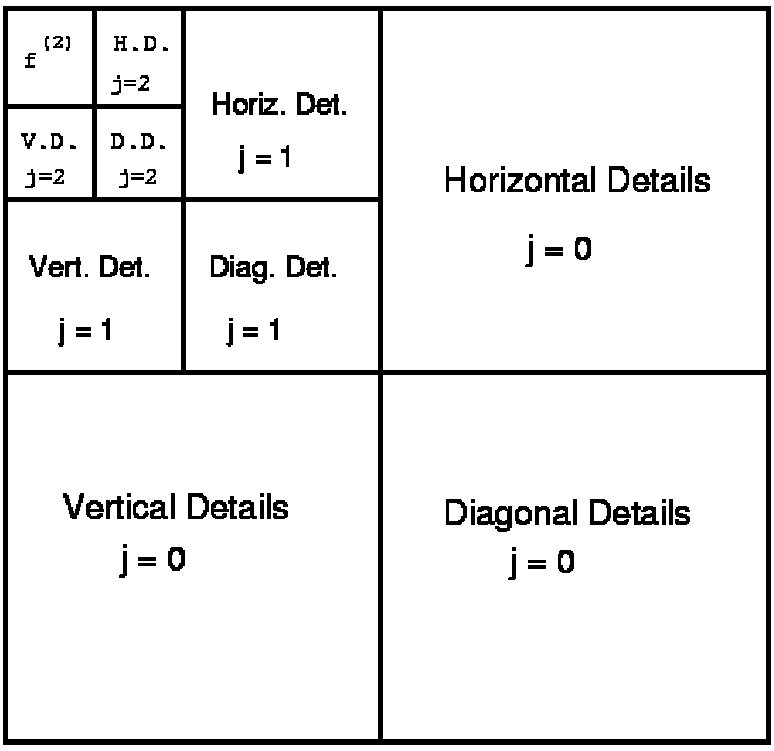


Figure 2.3: DWT of a two dimensional signal

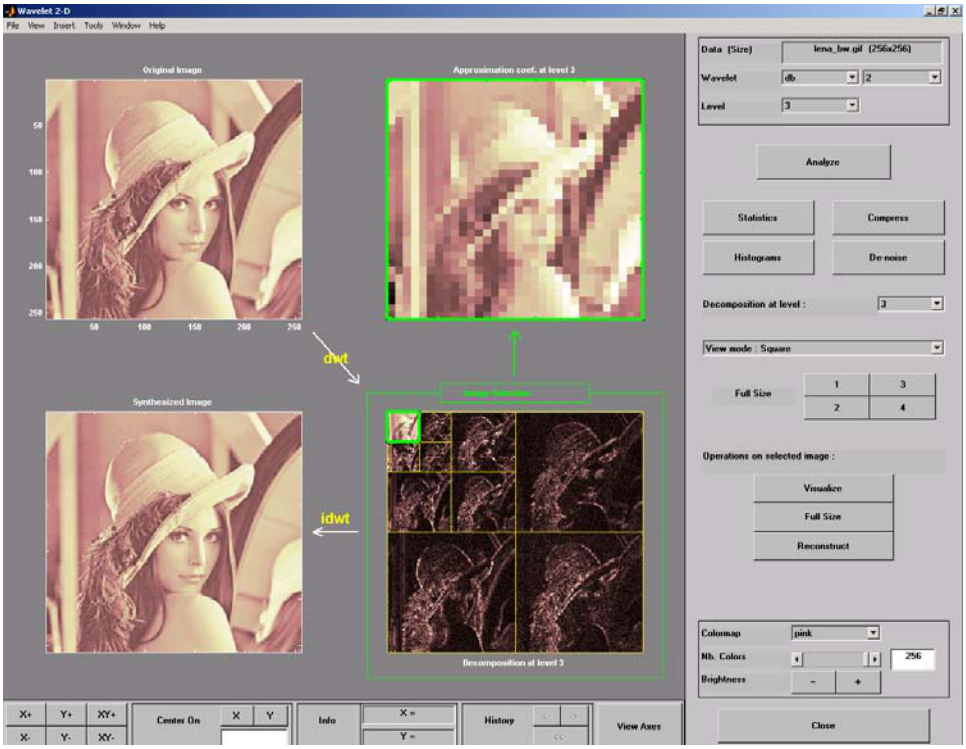


Figure 2.4: DWT of Lenna image

## 2.8 VANISHING MOMENTS

Any wavelet $\psi(x)$ that comes from the MRA must satisfy

$$\int_{\Re} \psi(x)dx = 0 \qquad (2.31)$$

The integral in the above equation is referred to as the zeroth moment of $\psi(x)$, so if the equation holds then we say that $\psi(x)$ has its zeroth moment vanishing. The integral $\int_{\Re} \psi^k(x)dx$ is referred as the $k^{\text{th}}$ moment of $\psi(x)$ and if $\int_{\Re} \psi^k(x)dx = 0$, we can say that $\psi(x)$ has its $k^{\text{th}}$ moment vanishing.

There are three important properties of the wavelets related to the number of its vanishing moments. The first property is smoothness. If $\{\psi_{j,k}(x)\}_{j,k\in Z}$ is an orthonormal

system on R and if $\psi(x)$ is smooth, then it will have vanishing moments. The smoother $\psi(x)$, the greater the number of vanishing moments. The second property is approximation. The wavelet series of a smooth function converges very rapidly to a function as long as the wavelet has a lot of vanishing moments. This means that relatively few wavelet coefficients are will be required in order to get a good approximation. In addition to that the wavelet is supported on a finite interval, so the function is smooth, which implies that more wavelet coefficients are required for a good approximation where the function is not smooth. The third property is the reproduction of polynomials. If $\psi(x)$ has compact support and N vanishing moments, then any polynomial of degree N-1 can be written as a linear combination of integer shift of the scaling function $\phi(x)$. If we consider a polynomial function *f(x)* of degree N-1 on the support of the wavelet $\{\psi_{j,k}(x)\}$, then $\langle f, \psi_{j,k} \rangle = 0$. This means that the non-zero wavelet coefficients of *f(x)* will only occur when the support $\{\psi_{j,k}(x)\}$ contains points of discontinuity of *f(x)*,i.e. a point where *f(x)* changes from one polynomial to another.

# CHAPTER 3

# EDGE DETECTION USING CLASICAL EDGE DETECTORS

Edge detection is one of the most important operations in image analysis. An edge is a set of connected pixels that lie on the boundary between two regions. The classification of edge detectors discussed in this chapter is based on the behavioral study of these edges with respect to the following operators:

- Gradient edge detectors
- Laplacian of Gaussian
- Gaussian edge detectors

## 3.1 GRADIENT EDGE DETECTORS

The first derivative assumes a local maximum at an edge. For a gradient image *f(x, y),* at location *(x, y),* where *x* and *y* are the row and column coordinates respectively, we typically consider the two directional derivatives. The two functions that can be expressed in terms of the directional derivatives are the gradient magnitude and the gradient orientation.

The gradient magnitude is defined by

$$|\nabla f| = \left\| \begin{bmatrix} G_x \\ G_y \end{bmatrix} \right\| = \left\| \begin{bmatrix} \frac{\partial f}{\partial x} \\ \frac{\partial f}{\partial y} \end{bmatrix} \right\| = \left[ G_x^2 + G_y^2 \right]^{\frac{1}{2}} \qquad (3.1)$$

This quantity give the maximum rate of increase of *f(x,y)* per unit distance in the gradient orientation of $|\nabla f|$. The gradient orientation is also an important quantity. The gradient orientation is given by

$$\angle \nabla f(x, y) = \tan^{-1}\left( \frac{G_y}{G_x} \right) \qquad (3.2)$$

where the angle is measured with respect to the x- axis. The direction of the edge at (x, y) is perpendicular to the direction of the gradient vector at that point. The other method of calculating the gradient is given by estimating the finite difference.

$$\frac{\partial f}{\partial x} = \lim_{h \to 0} \frac{f(x+h, y) - f(x, y)}{h} \qquad (3.3)$$

$$\frac{\partial f}{\partial y} = \lim_{h \to 0} \frac{f(x, y+h) - f(x, y)}{h}$$

therefore we can approximate this finite difference as

$$\frac{\partial f}{\partial x} = \frac{f(x+h, y) - f(x, y)}{h_x} = f(x+1, y) - f(x, y), (h_x = 1) \qquad (3.4)$$

$$\frac{\partial f}{\partial y} = \frac{f(x+h, y) - f(x, y)}{h_y} = f(x, y+1) - f(x, y), (h_y = 1) \quad (3.5)$$

Using the pixel coordinate notation and considering that *j* corresponds to the direction of *x* and *i* corresponds to the *y* direction

$$\frac{\partial f}{\partial x} = f(i, y+1) - f(i, j) \quad (3.6)$$

$$\frac{\partial f}{\partial y} = f(i-1, y) - f(i, j) \text{ or } \frac{\partial f}{\partial y} = f(i, j) - f(i+1, j) \quad (3.7)$$

The most popular classical gradient-based edge detectors are Roberts cross gradient operator, Sobel operator and the Prewitt operator.

### 3.1.1 ROBERTS EDGE DETECTOR

The calculation of the gradient magnitude and gradient magnitude of an image is obtained by the partial derivatives $\frac{\partial f}{\partial x}$ and $\frac{\partial f}{\partial y}$ at every pixel location. The simplest way to implement the first order partial derivative is by using the Roberts cross gradient operator.

Therefore

$$\frac{\partial f}{\partial x} = f(i, j) - f(i+1, j+1) \quad (3.8)$$

$$\frac{\partial f}{\partial y} = f(i+1, j) - f(i, j+1) \quad (3.9)$$

The above partial derivatives can be implemented by approximating them to two 2x2 masks. The Roberts operator masks are

$$G_x = \begin{bmatrix} -1 & 0 \\ 0 & 1 \end{bmatrix} \qquad G_y = \begin{bmatrix} 0 & -1 \\ 1 & 0 \end{bmatrix}$$

These filters have the shortest support, thus the position of the edges is more accurate, but the problem with the short support of the filters is its vulnerability to noise. It also produces very weak responses to genuine edges unless they are very sharp.

### 3.1.2 PREWITT EDGE DETECTOR

The Prewitt edge detector is a much better operator than the Roberts operator. This operator having a 3x3 masks deals better with the effect of noise.
An approach using the masks of size 3x3 is given by considering the below arrangement of pixels about the pixel *[i, j]*

$$\begin{matrix} a_o & a_1 & a_2 \\ a_7 & [i,j] & a_3 \\ a_6 & a_5 & a_4 \end{matrix}$$

The partial derivatives of the Prewitt operator are calculated as

$$G_x = (a_2 + ca_3 + a_4) - (a_0 + ca_7 + a_6) \qquad (3.10)$$

$$G_y = (a_6 + ca_5 + a_4) - (a_0 + ca_1 + a_2) \qquad (3.11)$$

The constant *c* implies the emphasis given to pixels closer to the center of the mask. $G_x$ and $G_y$ are the approximations at *[i, j]*.

Setting c = 1, the Prewitt operator is obtained. Therefore the Prewitt masks are as follows

$$G_x = \begin{bmatrix} -1 & -1 & -1 \\ 0 & 0 & 0 \\ 1 & 1 & 1 \end{bmatrix} \qquad G_y = \begin{bmatrix} -1 & 0 & 1 \\ -1 & 0 & 1 \\ -1 & 0 & 1 \end{bmatrix}$$

These masks have longer support. They differentiate in one direction and average in the other direction, so the edge detector is less vulnerable to noise.

### 3.1.3 SOBEL EDGE DETECTOR

The Sobel edge detector is very much similar to the Prewitt edge detector. The difference between the both is that the weight of the center coefficient is 2 in the Sobel operator. The partial derivatives of the Sobel operator are calculated as

$$G_x = (a_2 + 2a_3 + a_4) - (a_0 + 2a_7 + a_6) \qquad (3.12)$$

$$G_y = (a_6 + 2a_5 + a_4) - (a_0 + 2a_1 + a_2) \qquad (3.13)$$

Therefore the Sobel masks are

$$G_x = \begin{bmatrix} -1 & -2 & -1 \\ 0 & 0 & 0 \\ 1 & 2 & 1 \end{bmatrix} \qquad G_y = \begin{bmatrix} -1 & 0 & 1 \\ -2 & 0 & 2 \\ -1 & 0 & 1 \end{bmatrix}$$

Although the Prewitt masks are easier to implement than the Sobel masks, the later has better noise suppression characteristics.

### 3.1.4 FREI-CHEN EDGE DETECTOR

The Frei-Chen edge detector is also a first order operation like the previously discussed operators. Edge detection using the Frei-Chen masks is implemented by mapping the intensity vector using a linear transformation and then detecting edges based on the edges based on the angle between the intensity vector and its projection onto the edge subspace. Frei-Chen edge detection is realized with the normalized weights.

Frei-Chen masks are unique masks, which contain all of the basis vectors. This implies that a 3x3 image area is represented with the weighted sum of nine Frei-Chen masks. Primarily the image is convolved with each of the nine masks. Then an inner product of the convolution results of each mask is performed.

The Frei-Chen are

$$G_1 = \frac{1}{2\sqrt{2}} \begin{bmatrix} 1 & \sqrt{2} & 1 \\ 0 & 0 & 0 \\ -1 & -\sqrt{2} & -1 \end{bmatrix} \quad G_2 = \frac{1}{2\sqrt{2}} \begin{bmatrix} 1 & 0 & 1 \\ \sqrt{2} & 0 & \sqrt{2} \\ 1 & 0 & 1 \end{bmatrix} \quad G_3 = \frac{1}{2\sqrt{2}} \begin{bmatrix} 0 & -1 & \sqrt{2} \\ 1 & 0 & -1 \\ -\sqrt{2} & 1 & 0 \end{bmatrix}$$

$$G_4 = \frac{1}{2\sqrt{2}}\begin{bmatrix} \sqrt{2} & -1 & 1 \\ -1 & 0 & 1 \\ 0 & 1 & -\sqrt{2} \end{bmatrix} \quad G_5 = \frac{1}{2}\begin{bmatrix} 0 & 1 & 0 \\ -1 & 0 & -1 \\ 0 & 1 & 0 \end{bmatrix} \quad G_6 = \frac{1}{2}\begin{bmatrix} -1 & 0 & 1 \\ 0 & 0 & 0 \\ 1 & 0 & -1 \end{bmatrix}$$

$$G_7 = \frac{1}{6}\begin{bmatrix} -1 & -2 & 1 \\ -2 & 4 & -2 \\ 1 & -2 & 1 \end{bmatrix} \quad G_8 = \frac{1}{6}\begin{bmatrix} -2 & 1 & -2 \\ 1 & 4 & 1 \\ -2 & 1 & -2 \end{bmatrix} \quad G_9 = \frac{1}{3}\begin{bmatrix} 1 & 1 & 1 \\ 1 & 1 & 1 \\ 1 & 1 & 1 \end{bmatrix}$$

The first four Frei-Chen masks above are used for edges and the next four are used for lines and the last mask is used to compute averages. For edge detection, appropriate masks are chosen and the image is projected onto it. The projection equations are given by

$$\cos \grave{e} = \sqrt{\frac{M}{S}} \qquad (3.14)$$

where $M = \sum_{k \in \{e\}} (f_s, f_k)^2$ and $S = \sum_{k=1}^{9} (f_s, f_k)^2$

## 3.2 LAPLACIAN OF GAUSSIAN (LOG)

The principle used in the Laplacian of Gaussian method is, the second derivative of a signal is zero when the magnitude of the derivative is maximum. The Laplacian of a 2-D function *f(x, y)* is defined as

$$(\nabla^2 f)(x, y) = \frac{\partial^2 f}{\partial x^2} + \frac{\partial^2 f}{\partial y^2} \qquad (3.15)$$

### 3.2.1 THE LOG OPERATOR

The two partial derivative approximations for the Laplacian for a 3x3 region are given as

$$\nabla^2 f = 4(a_8) - (a_1 + a_3 + a_5 + a_7) \qquad (3.16)$$

$$\nabla^2 f = 8(a_8) - (a_0 + a_1 + a_2 + a_3 + a_4 + a_5 + a_6 + a_7) \qquad (3.17)$$

The masks for implementing these two equations are as follows

$$G_x = \begin{bmatrix} 0 & -1 & 0 \\ -1 & 4 & -1 \\ 0 & -1 & 0 \end{bmatrix} \qquad G_y = \begin{bmatrix} -1 & -1 & -1 \\ -1 & 8 & -1 \\ -1 & -1 & -1 \end{bmatrix}$$

The above partial derivative equations are isotropic for rotation increments of $90^0$ and $45^0$, respectively. Edge detection is done by convolving an image with the Laplacian at a given scale and then mark the points where the result have zero value, which is called the zero-crossings. These points should be checked to ensure that the gradient magnitude is large. Marr and Hildreth develop this method.

#### *Marr and Hildreth method*

The edge pixels in an image are determined by a single convolution operation. The basic principle of this method is to find the position in an image where the second derivatives become zero. These positions correspond to edge positions. The Gaussian function firstly smoothens or blurs any edge as shown in the figure 3.1. Blurring is

advantageous here because Laplacian would be *infinity* at unsmoothed edge and therefore edge position is still preserved. LOG operator is still susceptible to noise, but by ignoring zero-crossings produced by small changes in image intensity can reduce the effects of noise.

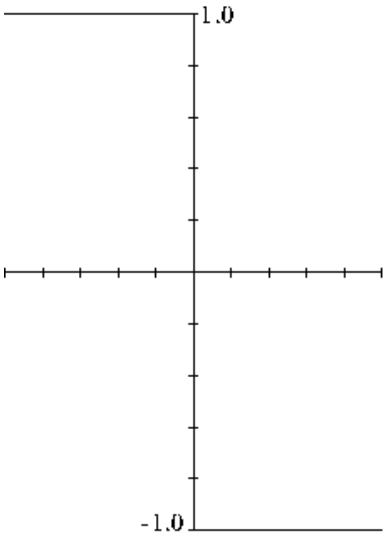


(a) *f(x)*

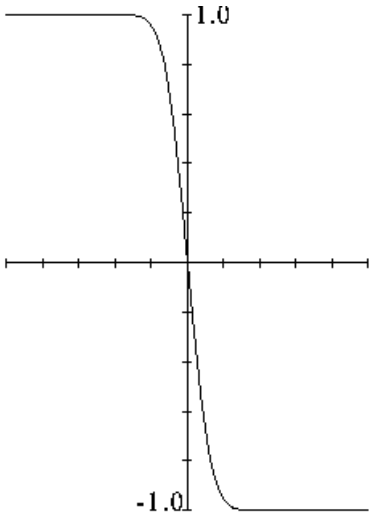


(b) Gaussian smoothing function of *f(x)*

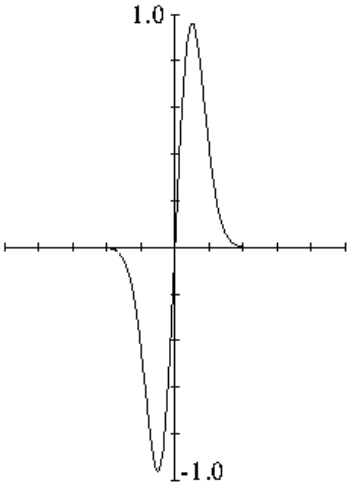


(c) Laplacian of Gaussian of *f(x)*

Figure 3.1: The smoothing of a signal with a Gaussian function

LOG operator gives edge direction information as well as edge points, determined from the direction of the zero-crossing. Hence the purpose of the Gaussian function in the LOG formulation is to smooth the image and the purpose of the Laplacian operator is to provide an image with zero crossings used to establish the location of edges. Some of the disadvantages of LOG are, the LOG being a second derivative operator the influence of noise is considerable. It always generates closed contours, which is not realistic. The Marr-Hildreth operator will mark edges at some locations that are not edges.

# CHAPTER 4

# ANALYSIS OF DIFFERENT WAVELET FAMILIES FOR EDGE DETECTION

## 4.1 DWT EDGE DETECTION

Significant intensity changes in an image normally occur at different spatial resolution or scales. Conventional edge detectors select a special spatial mask that detects edges at a particular resolution. A small mask edge detector is susceptible to noise and produces spurious edges. In contrast, to that a large mask edge detector is relatively robust to noise, but distorts the edges and may not detect some finer details. Thus it is very difficult to detect edges with a single spatial edge mask.

The edge preserved denoising lends itself to a wavelet-based procedure for edge detection. The edge in a signal gives rise to peaks in the high pass filter outputs or the detail subbands at concordant locations. This is a characteristic of the DWT. In other words, edges give rise to peaks across several levels of details at coordinate values that moves to the left by a factor of one half at every transition from a finer scale to a coarser scale. The stronger the edge, the higher are the peaks in the DWT. Consequently, an edge can be found from the wavelet transform by identifying peaks at concordant locations.

The wavelet transform of *f(x)* at the scale s and position *x* , computed with respect to the wavelet $\psi^a(x)$ is defined by

$$W_s^a f(x) = f * \psi_s^a(x) \qquad (4.1)$$

The wavelet transform with respect to $\psi^b(x)$ is

$$W_s^b f(x) = f * \psi_s^b(x) \qquad (4.2)$$

Therefore we derive that

$$W_s^a f(x) = s\frac{d}{dx}(f * \theta_s)(x) \qquad (4.3)$$

$$W_s^b f(x) = s^2\frac{d^2}{dx^2}(f * \theta_s)(x) \qquad (4.4)$$

The wavelet transforms $W_s^a f(x)$ and $W_s^a f(x)$ are, respectively, the first and second order derivatives of the signal smoothed at the scale *s*. The 2-D smoothing function is defined as any function $\theta(x, y)$ whose integral over *x* and *y* is equal to 1 and converges to 0 at infinity. The image *f(x, y)* is smoothed at different scales *s* by a convolution with $\theta_s(x, y)$. The gradient vector computed is given by $\vec{\nabla}(f * \theta_s)(x, y)$. Edges are defined as points $(x_0, y_0)$ where the modulus of the gradient vector is maximum in the direction towards which the gradient vector points in the image plane.

We define the two wavelet functions as

$$\psi^1(x,y) = \frac{\partial\theta(x,y)}{\partial x} \tag{4.5}$$

$$\psi^2(x,y) = \frac{\partial\theta(x,y)}{\partial y} \tag{4.6}$$

Let $\psi_s{}^1(x,y) = \frac{1}{s^2}\psi^1(\frac{x}{s},\frac{y}{s})$, $\psi_s{}^2(x,y) = \frac{1}{s^2}\psi^2(\frac{x}{s},\frac{y}{s})$ and $f(x,y) = L^2(R^2)$. Therefore

the wavelet transforms are as defined above are

$$W_s^1 f(x) = f * \psi_s^1(x,y) \tag{4.7}$$

$$W_s^2 f(x) = f * \psi_s^2(x,y) \tag{4.8}$$

Therefore we prove that

$$\begin{pmatrix} W_s^1 f(x,y) \\ W_s^2 f(x,y) \end{pmatrix} = s\vec{\nabla}(f * \theta_s)(x,y) \tag{4.9}$$

Hence the edge points can be located from the components $W_s^1 f(x)$ and $W_s^2 f(x)$ of the wavelet transform.

## 4.2 HAAR WAVELET

The two functions that play an important role in wavelet analysis are the scaling function $\phi$ and the wavelet $\psi$. These functions generate a family of functions that can be used to break up or reconstruct a signal. $\phi$ is also called the father wavelet and $\psi$ is called the mother wavelet. The Haar wavelet is the first known wavelet and was proposed in 1909 by Alfred Haar. The Haar wavelet is also the simplest possible wavelet.

### 4.2.1 HAAR SCALING FUNCTION

The simplest wavelet analysis is based on the Haar scaling function. The Haar scaling function is defined as

$$\phi(x) = \begin{cases} 1, if\ 0 \le x < 1 \\ 0, elsewhere \end{cases} \qquad (4.10)$$

The father wavelet is also known as the characteristic function of the unit interval. The Haar scaling function is shown in the figure 4.1.

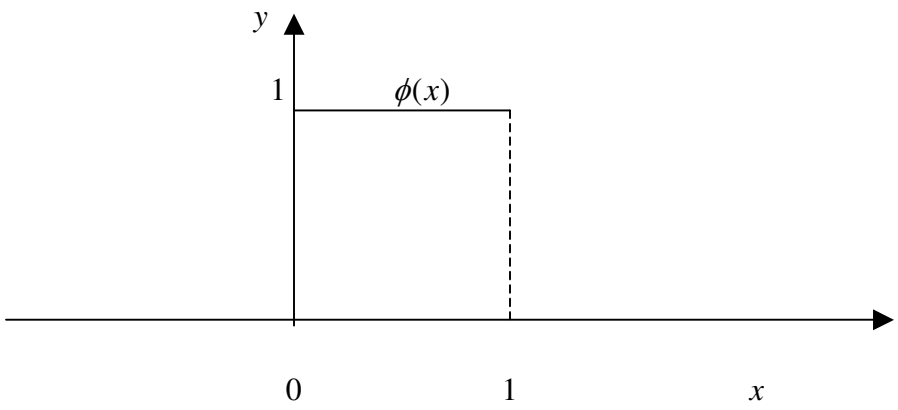


Figure 4.1: graph of $\phi(x)$

The function of $\phi(x-k)$ has the similar graph as of $\phi(x)$ but translated to the right by $k$ units. Let $V_0$ be the space of all functions of the form

$$\sum_{k\in Z} a_k \phi(x-k) \quad a_k \in \Re$$

where $k$ range over any finite set of integers. $V_0$ consists of all piecewise constant functions as $\phi(x-k)$ is discontinuous at $x=k$ and $x=k+1$. Since k ranges over a finite set, can each element of $V_0$ is zero outside a bounded set, this function is called as finite or compact support.

The basic properties of a Haar scaling function are that a function *f(x)* belongs to $V_0$ if and only if $f(2^j x)$ belongs to $V_j$ and f(x) belongs to $V_j$ if and only if $f(2^{-j} x)$ belongs to $V_0$. The set of functions $2^{\frac{j}{2}} h(2^j x-k)\,;\ k \in Z$ is an orthonomal basis of $V_j$.

### 4.2.2 CONSTRUCTION OF HAAR WAVELET

Two factors influencing the construction of $\psi$ are

1. $\psi$ is a member of $V_1$ and so $\psi$ can be expressed as $\sum_l a_l \phi(2x-l)$ for $a_l \in \Re$.
2. $\psi$ is orthogonal to $V_0$. This is equivalent to $\int \psi(x)\phi(x-k)dx = 0$ for all integers *k.*

The simplest $\psi$ satisfying both these factors is shown in the figure below. This graph consists of two blocks of width one-half and can be expressed as

$$\psi(x) = \phi(2x) - \phi(2(x-1/2)) = \phi(2x) - \phi(2x-1) \qquad (4.11)$$

Thus satisfying the definition of the wavelet

$$\int_{-\infty}^{\infty} \phi(x)\psi(x)dx = \int_{0}^{\frac{1}{2}} 1dx - \int_{\frac{1}{2}}^{1} 1dx = 0 \qquad (4.12)$$

Thus, $\psi$ is orthogonal to $\phi$. If $k \neq 0$, then the support of $\psi(x)$ and the support of $\phi(x-k)$ do not overlap and so $\int \psi(x)\phi(x-k)dx = 0$. Therefore, $\psi$ belongs to $V_1$ and is orthogonal to $V_0$. Thus $\psi$ is called the Haar wavelet and is shown in figure 4.2.

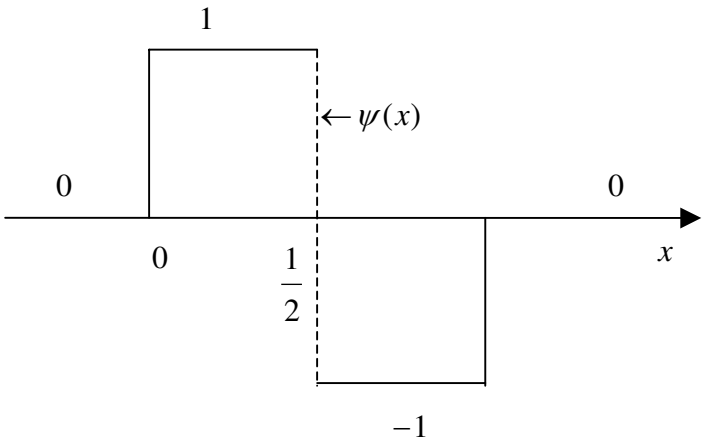


Figure 4.2: The Haar wavelet

The Haar wavelet (mother wavelet) is the function, which we shall indicate with H, is the function that is defined by

$$\psi(x) = \begin{Bmatrix} 1, if\ 0 \le x < \frac{1}{2} \\ -1, if\ \frac{1}{2} \le x < 1 \\ 0, elsewhere \end{Bmatrix} \qquad (4.13)$$

The Haar wavelet is a function

$$\psi(x) = \phi(2x) - \phi(2x-1) \qquad (4.14)$$

The family of wavelets is given by $h_{j,k}(x) = 2^{\frac{j}{2}} h(2^j x - k)$. The collection of $\{h_{j,k}(x)\}_{j,k \in Z}$ is referred to as the Haar system on R. for each $j \in Z$, and the collection $\{h_{j,k}(x)\}_{k \in Z}$ is referred to as the system of scale *j* Haar function.

### 4.2.3 DISCRETE HAAR TRANSFORM

Given $J, N \in N$ with $J < N$ and a finite sequence $c_0 = \{c_0(k)\}_{k=0}^{2^N - 1}$, the discrete Haar transform is defined as

$$\{d_j(k) : 1 \le j \le J; 0 \le k \le 2^{N-j} - 1\} \cup \{c_j(k) : 0 \le k \le 2^{N-J} - 1\} \qquad (4.15)$$

Where

$$c_j(k) = \frac{1}{\sqrt{2}} c_{j-1}(2k) + \frac{1}{\sqrt{2}} c_{j-1}(2k+1) \qquad (4.16)$$

$$d_j(k) = \frac{1}{\sqrt{2}} c_{j-1}(2k) - \frac{1}{\sqrt{2}} c_{j-1}(2k+1) \qquad (4.17)$$

The inverse DHT is given by

$$c_{j-1}(2k) = \frac{1}{\sqrt{2}} c_j(k) + \frac{1}{\sqrt{2}} d_j(k) \qquad (4.18)$$

$$c_{j-1}(2k+1) = \frac{1}{\sqrt{2}} c_j(k) - \frac{1}{\sqrt{2}} d_j(k) \qquad (4.19)$$

DHT can be thought of as a linear transformation on a finite-dimensional space and can be written as multiplication by a matrix.

Given that $L \in \mathrm{N}$ even, we can define the *(L / 2) x L* matrices $H_L$ and $G_L$ as

$$H_L = \frac{1}{\sqrt{2}} \begin{pmatrix} 1 & 1 & 0 & & \dots & & 0 \\ 0 & 0 & 1 & 1 & 0 & \dots & 0 \\ & & & \vdots & & & \\ 0 & & \dots & & 0 & 1 & 1 \end{pmatrix} \qquad (4.20)$$

$$G_L = \frac{1}{\sqrt{2}} \begin{pmatrix} 1 & -1 & 0 & & \dots & & 0 \\ 0 & 0 & 1 & -1 & 0 & \dots & 0 \\ & & & \vdots & & & \\ 0 & & \dots & & 0 & 1 & -1 \end{pmatrix} \qquad (4.21)$$

Therefore we define the *L x L* matrix $W_L$ by

$$W_L = \begin{pmatrix} H_L \\ G_L \end{pmatrix} \qquad (4.22)$$

The matrix $H_L$ is referred to as the approximation matrix and the matrix $G_L$ as the detail matrix, and the matrix $W_L$ as the wavelet matrix. The identity matrix *I* is given by $I = H * H + G * G$.

### 4.2.4 DHT IN TWO DIMENTIONS

The DHT to two dimensional signals involves the separate application of the ordinary DHT to the rows and columns of the signal.

Considering $L \in$ N , let H and G be the (L / 2) x L matrices. Let c be an M x L matrix of the form

$$c = \begin{pmatrix} c_0 \\ c_1 \\ c_2 \\ \cdots \\ c_{M-1} \end{pmatrix} \qquad (4.23)$$

Therefore we can define the row-wise approximation matrix of c, $H^{row}c$ to be the M x (L / 2)

$$H^{row}c = \begin{pmatrix} Hc_0 \\ Hc_1 \\ Hc_2 \\ \cdots \\ Hc_{M-1} \end{pmatrix} \qquad (4.24)$$

Similarly we can define the row-wise detail matrix of c, $G^{row}c$ as

$$G^{row}c = \begin{pmatrix} Gc_0 \\ Gc_1 \\ Gc_2 \\ \cdots \\ Gc_{M-1} \end{pmatrix} \qquad (4.25)$$

If we consider $c$ be an M x L matrix of the form

$$c = \begin{pmatrix} c_0 & c_1 & c_2 & \cdots & c_{M-1} \end{pmatrix} \qquad (4.26)$$

The column-wise approximation matrix and the column-wise detail matrix of c, $H^{col}c$ and $G^{col}c$ are defined to be

$$H^{col}c = \begin{pmatrix} Hc_0 & Hc_1 & Hc_2 & \cdots & Hc_{M-1} \end{pmatrix} \qquad (4.27)$$

$$G^{col}c = \begin{pmatrix} Gc_0 & Gc_1 & Gc_2 & \cdots & Gc_{M-1} \end{pmatrix} \qquad (4.28)$$

### 4.2.5 EDGE DETECTION USING HAAR WAVELET

Each pixel in an image has 8 other neighboring pixels, two in the horizontal direction, two in the vertical direction and four in the diagonal direction. If at a given location, the variation of the pixel value is small in the vertical direction but large in the horizontal direction, then the pixel is a vertical edge point of the image. Similarly if the variations in the horizontal direction pixel values are smaller and the vertical direction pixel vales are larger, then the pixel is a horizontal edge point. If the variations in the

pixel values of both the horizontal and the vertical are large, then the pixel is a diagonal edge point of the image.

Since the DHT of matrices involves computing averages and differences of adjacent pixel values in various combinations, we can find the edges in an image using the DHT.

If we consider a $2^{N-1} \times 2^{N-1}$ matrix $d_1^{(1)}$ derived from an image $c_0 = \{c_0(n,m)\}_{m,n=0}^{2^N-1}$ for $0 \le n, m \le 2^{N-1}$. As we know that $d_1^{(1)} = G_{2^n}^{col} H_{2^N}^{row} c_0$

Therefore

$$d_1^{(1)} = \frac{1}{2}(c_0(2n,2m) - c_0(2n+1,2m)) + \frac{1}{2}(c_0(2n,2m+1) - c_0(2n+1,2m+1)) \quad (4.29)$$

If (*2n, 2m*) is a horizontal edge point of the image $c_0$, then the difference $(c_0(2n,2m) - c_0(2n+1,2m))$ and $(c_0(2n,2m+1) - c_0(2n+1,2m+1))$ will tend to a large value due to the large variation in pixel values in the vertical direction. If (*2n, 2m*) is a vertical edge point, then these same differences will tend to be close to zero. If (*2n, 2m*) is a diagonal edge point, then the pixel values will tend to be a similar to one of the diagonal directions or one of the differences tends to zero.

Since the matrix $c_j$ can be thought of as containing the features of the original image that are of the size $2^j$ or larger, the matrices $d_j^{(1)}, d_j^{(2)}$, and $d_j^{(3)}$ are called the horizontal, vertical and diagonal edges, respectively, at scale $2^j$.

## 4.3 DAUBECHIES WAVELET

The Haar and Shannon scaling functions are the two extremes. The Haar father wavelet has compact support but is discontinuous. On the other hand, the Shannon scaling function is smooth and continuous but extends through out the whole real line i.e. the support is all of R. Since these wavelets are the two extremes of support and continuity spectra, neither of them is useful for the applications.

Ingrid Daubechies discovered a wavelet in 1987 that is a sort of compromise between compact support and smoothness. The Daubechies wavelet transform is similar to that of Haar i.e. by computing running averages and differences via scalar products with scaling signals and wavelets. The only difference between them consists in how these scaling signals and wavelets are defined. For the Daubechies wavelet transform the scaling signals and the wavelets produce averages and differences using more number of values from the signal. These slight changes produce a great improvement in the capability of the new transform.

### 4.3.1 CONSTRUCTION OF DAUBLETS

If $\{\psi_{j,k}(x)\}$ is an orthonormal wavelet basis, and the wavelet $\psi(x)$ is smooth, then it must have vanishing moments. The smoother the wavelet, the more moments that must vanish. The Daubechies wavelets have the largest number of vanishing moments for their support. For each $N \in \mathrm{N}$, the Daubechies wavelet of order $N$ has $N$ vanishing moments and is supported on the interval [0, 2$N$-1]. The Daubechies wavelets as shown in figure 4.3 become smoother with increasing $N$.

Let $\varphi(x)$ be a compactly supported scaling function associated with an MRA with finite scaling filter *h(n)*. Let $\psi(x)$ be the corresponding wavelet given by

$$\psi(x) = \sum_k g(k) 2^{\frac{1}{2}} \varphi(2x-k) \qquad (4.30)$$

Then for each $N \in \mathrm{N}$, the following are defined.

1. $\int_{\Re} x^k \psi(x) dx = 0 \quad for 0 \le k \le N-1.$ *(4.31)*

2. $m_0^{(k)}(1/2) = 0, \quad for 0 \le k \le N-1.$ *(4.32)*

3. $m_0(\omega)$ can be factored as

$$m_0(\omega) = \left( \frac{1+e^{-2\pi i\omega}}{2} \right)^N L(\omega) \qquad (4.33)$$

for some period, *L* is a trigonometric polynomial

4. $\sum_n h(n)(-1)^n n^k = 0 \quad for 0 \le k \le N-1.$ *(4.34)*

To find a finite scaling filter *h(k)* of length *2N*, a trigonometric polynomial of the form

$$m_0(\omega) = \frac{1}{\sqrt{2}} \sum_k h(k) e^{-2\pi i k\omega} \qquad (4.35)$$

For the orthonormality condition to be satisfied

$$L(\omega) = \left| L(\omega) \right|^2 = P(\sin^2 \frac{\omega}{2}) \qquad (4.36)$$

Where

$$P(y) = P_N(y) + y^N R(\frac{1}{2} - y) \qquad (4.37)$$

$$P_N(y) = \sum_{k=0}^{N-1} \binom{N-1+k}{k} y^k \qquad (4.38)$$

and $R$ is an odd polynomial *(f(-x) = -f(x))* that ensures $P(y) \geq 0$ when $y \in [0,1]$. The polynomial $P_{N-1}(y)$ is the degree *N-1* polynomial and can be defined as

$$P_{N-1}(y) = \sum_{k=0}^{N-1} \binom{2N-1}{k} y^k (1-y)^{N-1-k} \qquad (4.39)$$

We can calculate the Daubechies scaling filters for different values of $N$ by using the above equations and formulae . The values of the scaling filer for *N=1* are given as

$$h(n) = \begin{cases} \dfrac{1}{\sqrt{2}} \\ 0 \end{cases} \begin{matrix} n = 0,1 \\ otherwise \end{matrix} \qquad (4.40)$$

The Daubechies scaling filters for *N=2* is calculated to be

$$m_0(\omega) = \frac{1}{\sqrt{2}} \sum_k h(k) e^{-ik\omega} = \left( \frac{1+e^{-i\omega}}{2} \right)^N L(\omega) \qquad (4.41)$$

$$= \frac{1+\sqrt{3}}{8} e^{-0i\omega} + \frac{3+\sqrt{3}}{8} e^{-1i\omega} + \frac{3-\sqrt{3}}{8} e^{-2i\omega} + \frac{1-\sqrt{3}}{8} e^{-3i\omega}$$

Therefore

$$h(0) = \frac{1+\sqrt{3}}{4\sqrt{2}},\ h(1) = \frac{3+\sqrt{3}}{4\sqrt{2}},\ h(2) = \frac{3-\sqrt{3}}{4\sqrt{2}},\ h(3) = \frac{1-\sqrt{3}}{4\sqrt{2}}$$

Once the coefficients, $h(k)$, have been found and $\phi$ has been constructed, then the wavelet $\psi$ associated with the Daubechies scaling function is given by the formula

$$\psi(x) = \sum_{k \in Z} (-1)^k h_{1-k} \phi(2x - k) \qquad (4.42)$$

Smoother scaling functions (as shown in figure 4.4) of higher and wavelets of higher order can be obtained by choosing a higher power for *N*.

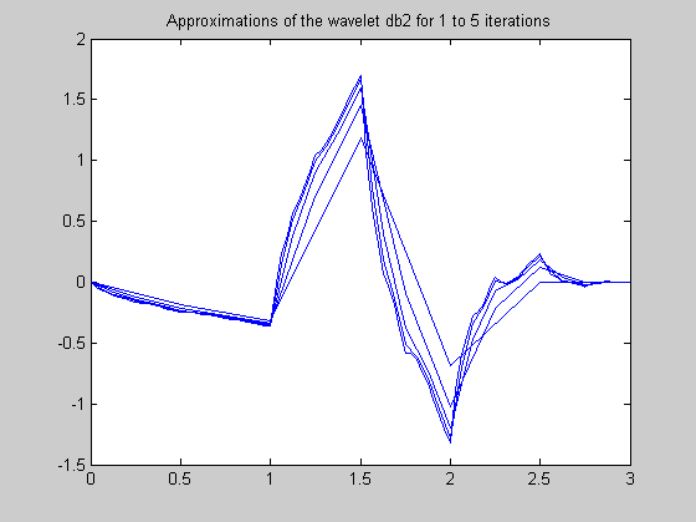


Figure 4.3: The approximation of db2 wavelet for 1 to 5 iterations

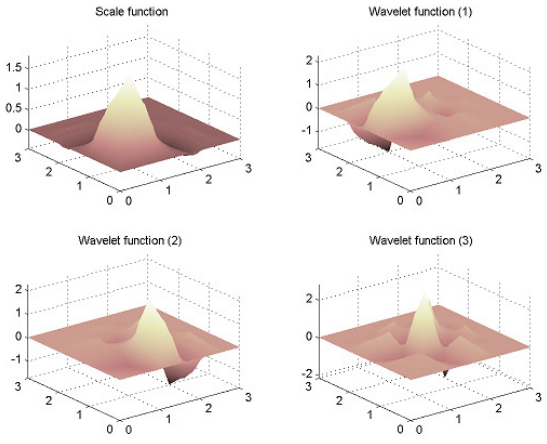


Figure 4.4: The approximations of the db2 wavelet and scale functions

### 4.3.2 2-D DAUBECHIES WAVELET TRANSFORM

For a square array $S = (s_{i,j})$ with $2^n$ rows and $2^n$ columns, similar to the Haar transform, one of Daubechies two dimensional wavelet transforms consists in performing a first pass on each row, from $(a_{i,j}^{(n)})_{j=0}^{2^n-1}$ to $(a_{i,j}^{(n-1)})_{j=0}^{2^{n-1}-1}$ and $(c_{i,j}^{(n-1)})_{j=0}^{2^{n-1}-1}$. Then it performs a first pass on each of the new column. The two dimensional Daubechies wavelet transform produces the coefficient of tensor product wavelets. The tensor products are

$$\phi_{k,l}^{(n-1)} = \varphi_k \otimes \varphi_l \text{ in the upper left hand corner of each 2 x 2 block} \quad (4.43)$$

$$\psi_{k,l}^{h,(N-1)} = \varphi_k \otimes \psi_l \text{ in the upper right hand corner of each 2 x 2 block} \quad (4.44)$$

$$\psi_{k,l}^{v,(N-1)} = \psi_k \otimes \varphi_l \text{ in the lower left hand corner of each 2 x 2 block} \quad (4.45)$$

$$\psi_{k,l}^{d,(N-1)} = \psi_k \otimes \psi_l \text{ in the lower right hand corner of each 2 x 2 block} \quad (4.46)$$

The next pass then repeats the first pass on the smaller array, with $2^{n-1}$ rows and $2^{n-1}$ columns, of the coefficients of each $\phi_{k,l}^{(n-1)}$ in the upper left hand corner of each 2 x 2 block. The decomposition and reconstruction filters of db2 are shown in figure 4.5.

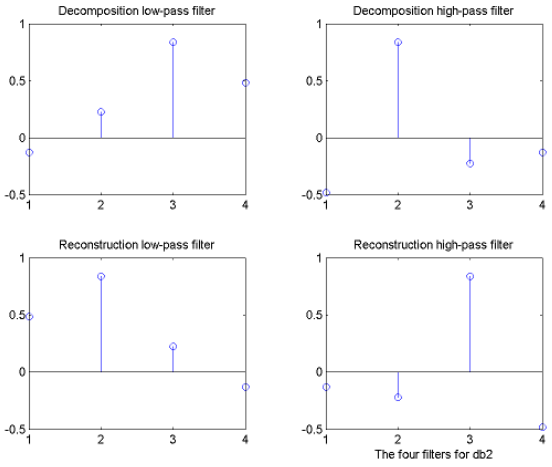


Figure 4.5: The decomposition and reconstruction filters of db2

### 4.3.3 EDGE DETECTION USING DAUBLETS

Consider a wavelet decomposition over and reconstruction over a single level. The LL band analysis filter produces a low pass filtered version of the edge. The output of the highpass filter corresponding to the orientation of the image containing a change in the location of the edge as well as further details. The other highpass filters yield only the details. In a highly compressed image the pixels in the subimages corresponding to high frequency bands are often lost. Thus the edge response of the system is to a large extent determined by the edge response of the LL filter. The edge response of the LL filter inherently contains ripples. If the compression rate is moderate, then the details in the subimages corresponding to the high frequency bands cancel the ripples due to the LL filter, thereby producing a smooth edge.

## 4.4 COIFMAN WAVELETS

Coifman wavelets are designed for the purpose of maintaining a close match between the trend values and the original signal values. Coiflets are another variation on Daubechies wavelets. Coiflets were first constructed by Daubechies. They are so named by Ingrid Daubechies because Ronald Coifman suggested the construction of orthonormal wavelet basis with vanishing moment conditions both for $\phi$ as well as for $\psi$.

Coiflets are orthogonal wavelets for which $\psi$ has several vanishing moments, and for which $\phi$ also has several vanishing moments. The idea is to find the form of $m_0(\omega)$ that satisfies the orthogonality condition and both moment conditions for $\phi$ and $\psi$. These moment conditions are

$$\int x^k \psi(x)dx = 0, \quad k = 0,\ldots,N-1 \qquad (4.47)$$

$$\int \phi(x)dx = 1, \tag{4.48}$$

$$\int x^k \phi(x)dx = 0\,, \quad k = 0,\ldots,N \tag{4.49}$$

These two moment conditions translate into the following conditions on $m_0(\omega)$

$$m_0^{(k)}(\pi) = 0 \quad \text{for } k = 0,\ldots,N-1 \tag{4.50}$$

and

$$m_0(0) = 0\ ,\ m_0^{(k)}(0) = 0 \text{ for } k = 0,\ldots,N-1$$

Therefore the following form of $m_0(\omega)$ fulfills both the moment conditions

$$m_0(\omega) = \left(\cos^2\frac{\omega}{2}\right)^L \left[\sum_{l=0}^{L-1}\binom{L-1+l}{l}\left(\sin^2\frac{\omega}{2}\right)^l + \left(\sin^2\frac{\omega}{2}\right)^L f(\omega)\right] \tag{4.51}$$

where $2L = N$ and $f(\omega)$ is chosen to be

$$f(\omega) = \sum_{n=0}^{2L-1} f_n e^{in\omega} \tag{4.52}$$

The coefficients $f(\omega)$ are determined by requiring $m_0(\omega)$ to satisfy the orthogonality condition.

To obtain the filters and wavelets commonly known as coiflets (as shown in figure 4.6) we require fewer alternating moments to be zero but require some moments to be zero i.e.

1. Normalization: $\sum_{n=0}^{L-1} h_0(n) = 1$ *(4.53)*

2. double shift orthogonality: $\sum_{n=0}^{L-1} h_0(n) h_0(n-2m) = 0.$ *(4.54)*

3. N alternate moments are zero: $\sum_{n=0}^{L-1} n^k (-1)^n h_0(n) = 0 \text{ for } k = 0,\ldots,N-1$ *(4.55)*

4. J moments are zero: $\sum_{n=0}^{L-1} n^k h_0(n) = 0 \text{ for } k = 0,\ldots,J$ *(4.56)*

We know that $H_0^{(k)}(0) = \sum_{n=0}^{L-1} \left(-2\pi j\right)^k n^k h_0(n)$ *(4.57)*

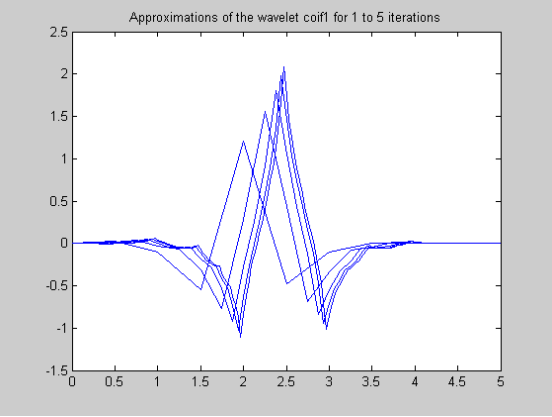


Figure 4.6: The approximation of the coif1 wavelet for 1 to 5 iterations

The result from simplifying the computation of the derivative of $\left|H_0(f)\right|^2$ at $f = 0$ is given as $\mu(k) = \frac{-1}{2\sqrt{2}} \sum_{i=1}^{k-1} \binom{k}{i} \mu(i)\mu(k-i)$. *(4.58)*

This shows that for k even, $\mu(k)$ can be written in terms of the odd lower order moments $\mu(i)$. If the odd moments $\mu(i)$ are zero for $i = 1,3,5,\ldots,J-1$ then all the even moments are zero too so that all the moments up to order *J* are zero.

If we chose K = 2 N and N = 6 I the following conditions are obtained

1. Normalization: $\sum_{n=0}^{L-1} h_0(n) = 1$

2. double shift orthogonality: $\sum_{n=0}^{L-1} h_0(n) h_0(n-2m) = 0.$

3. K = 2 I = N/3 alternate moments are zero: $\sum_{n=0}^{L-1} n^k (-1)^n h_0(n) = 0$ for $k = 0,\ldots,2N-1$

4. K = 2 I = N / 3 moments are zero: $\sum_{n=0}^{L-1} n^k h_0(n) = 0$ for $k = 1,3,5,\ldots,2N-1$

This set of conditions leads to the coifI filter and wavelet. The filter has length 6 N and 2 I zero alternating moments and 2 N zero moments. The decomposition and reconstruction filters of the coiflets are shown in figure 4.8.

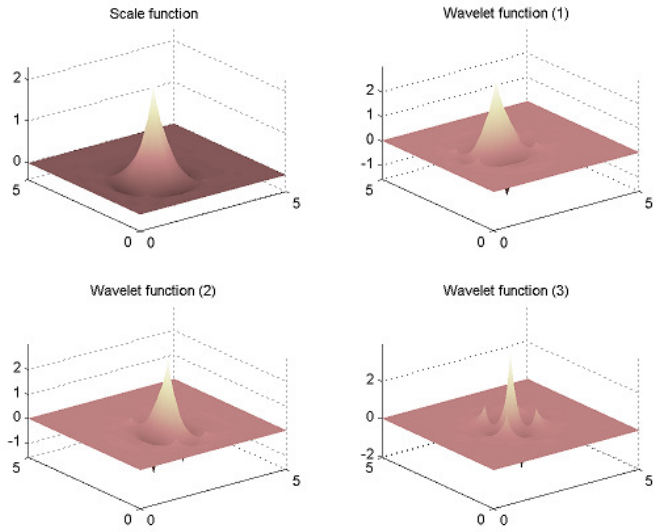


Figure 4.7: The approximations of the coif1 wavelet and scale functions

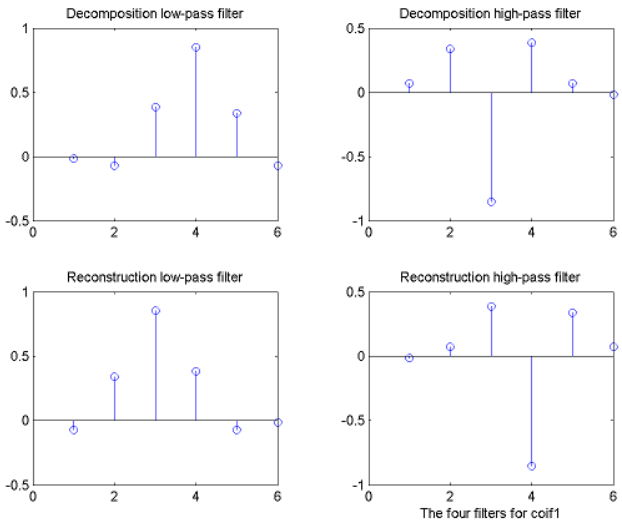


Figure 4.8: The decomposition and reconstruction filters of coif1

## 4.5 BIORTHOGONAL WAVELETS

Biorthogonal wavelets are symmetric wavelets with compact support unlike Daubechies wavelets which are asymmetric. Biorthogonal wavelets provide perfect reconstruction of the signal, without redundancy, using two sets of wavelets. One set of wavelets is used for the decomposition and the other is used for reconstruction.

### 4.5.1 CONSTRUCTION OF BIORTHOGONAL WAVELETS

Consider the dilation and translation of the scaling function $\{\phi_{j,k}(x)\}$ constitutes the basis for $V_j$, similarly $\{\psi_{j,k}(x)\}$ constitutes a basis for $W_j$. Let the dual subspaces $\tilde{V}_j$ and $\tilde{W}_j$ be generated from a dual scaling function $\tilde{\phi}$ and a dual mother wavelet $\tilde{\psi}$. Therefore the conditions for biorthogonality as proven by Cohen, Daubechies and Jawerth and Sweldens are

$$\left\langle \phi_{jl}, \tilde{\phi}_{jk} \right\rangle = \delta_{lk} \quad \text{and} \quad \left\langle \psi_{j'l}, \tilde{\psi}_{jk} \right\rangle = \delta_{lk}\delta_{jj'} \tag{4.59}$$

and

$$\left\langle \phi_{jl}, \tilde{\psi}_{jk} \right\rangle = 0 \text{ and } \quad \left\langle \psi_{jl}, \tilde{\phi}_{jk} \right\rangle = 0 \tag{4.60}$$

Where $\tilde{\phi}_{j,k}(x) = 2^{\frac{j}{2}} \tilde{\phi}(2^j x - k)$ and $\tilde{\psi}_{j,k}(x) = 2^{\frac{j}{2}} \tilde{\psi}(2^j x - k)$. $\psi$ and $\tilde{\psi}$ are called as biorthogonal wavelets (shown in figure 4.9). The biorthogonality condition in the form of space are given as

$V_j \perp \tilde{W}_j$, $\tilde{V}_j \perp W_j$, and $W_j \perp \tilde{W}_j$ for $j \neq j'$.

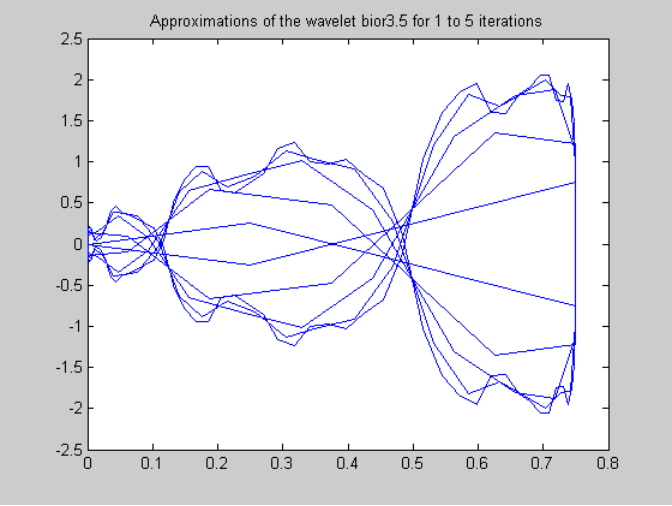


Figure 4.9: The approximation of the bior3.5 wavelet for 1 to 5 iterations

### 4.5.2 PROPERTIES OF BIORTHOGONAL WAVELETS

Biorthogonal wavelets have the smallest supported set. They are capable of detecting singular data. its has the two way capability, one is to smooth data with a B-spline scaling function and another is to detect distributed data with biorthogonal wavelets. So this specific property provides the foundation for image edge detection based on the biorthogonal wavelet transform. Three degree biorthogonal wavelets are used to detect edges in an image. The wavelet bases constructed by the biorthogonal wavelet functions translation and dilation are semi-orthogonal wavelet bases. Therefore these wavelets are orthogonal to scaling functions at the same level but not orthogonal to each other.

### 4.5.3 EDGE DETECTION USING BIORTHOGONAL WAVELETS

The image is decomposed into four weights, $S_{2^j} f(x,y), W_{2^j}^h f(x,y)$, $W_{2^j}^v f(x,y)$ and $W_{2^j}^d f(x,y)$ at scale $2^j$. $S_{2^j} f(x,y)$ is called the discrete approximation signal of image while $W_{2^j}^h f(x,y)$, $W_{2^j}^v f(x,y)$ and $W_{2^j}^d f(x,y)$ are called the discrete detail signal of image.

The local maxima in the position of horizontal detail image $W_{2^j}^h f(x,y)$ and vertical detail image $W_{2^j}^v f(x,y)$ is corresponding to the image edge point in horizontal and vertical direction. At the scale $2^j$, the value of $M_{2^j} f(x,y)$ is $\sqrt{\left|W_{2^j}^h f(x,y)\right|^2 + \left|W_{2^j}^v f(x,y)\right|^2}$. The local maxima point means that this point value $M_{2^j} f(x,y)$ is larger than of these closed points. The edge of the image can be detected at every scale. When the scale of the biorthogonal wavelet increases the ability of reducing the noise increases.

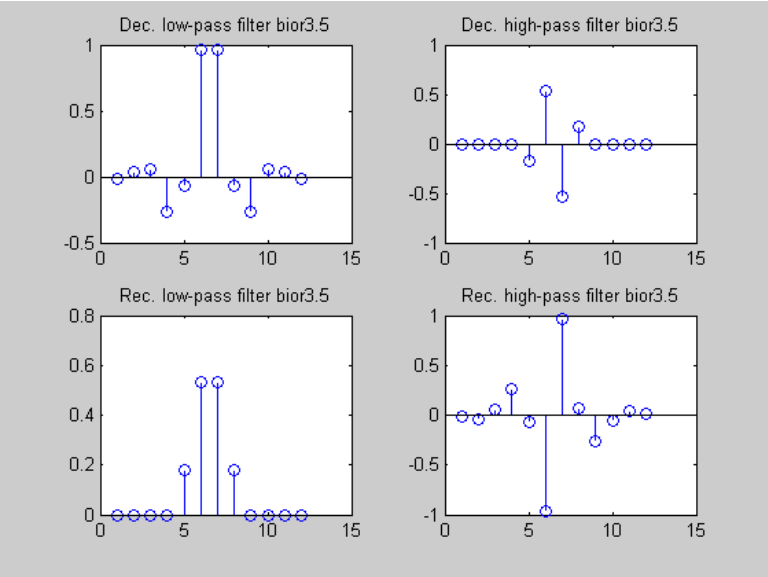


Figure 4.10: The decomposition and reconstruction filters of bior 3.5

# CHAPTER 5

# RESULTS OF EDGE DETECTION AND DEVELOPMENT OF MULTISCALE WAVELET EDGE DETECTION

## 5.1 TRADITIONAL EDGE DETECTION OF IMAGE WITHOUT NOISE

Figure 5.1 shows the edge detection of lenna image using the gradient edge detection techniques like Robert, Prewitt, Sobel and Frei-Chen operators. Figure 5.1(a) shows the noise free image of lenna. The image of lenna has 256 x 256 pixels. The contour map of the lenna image in figure 5.1(a) is shown in figure 5.1(b). The ideal edge detector should follow the edges in the figure 5.1(b).

Edge detection with Robert operator is shown in figure 5.1(c). A better edge detection of the lenna image is shown in figure 5.1(d) where a Prewitt operator and 5.1(e) where a Sobel operator is used. Most of the edge detectors work well with noiseless images. The superiority of advanced edge detectors is clearly shown when edge detection is performed on a noisy image. A more complicated and better edge detector is shown in figure 5.1(f). The Frei-Chen edge operator shown in figure 5.1(f) uses 9 masks for edge detection. It reveals that it is a better edge detection operator for a noiseless image when compared with other gradient operators.

(a)

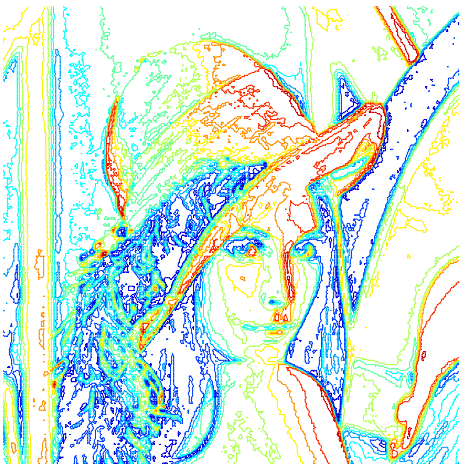

(b)

(c)

(d)

(e)

(f)

Figure 5.1: Edge detection of noiseless lenna image using gradient edge detectors (a) Original noiseless lenna image (b) Contour image of lenna (c) Robert edge detection (d) Prewitt edge detection (e) Sobel edge detection (f) Frei-Chen edge detection

Gradient operation is an effective detector for sharp edges where the pixel gray levels change over space very rapidly. But when the gray levels change slowly from dark to bright, the gradient operation will produce a very wide edge. It is helpful in this case to consider using the Laplace operation. The second order derivative of the wide edge will have a zero crossing in the middle of edge. Figure 5.2 shows the edge detection using LOG operator. The edge detection result of lenna shown in figure 5.2(a) using the LOG technique is visualized in figure 5.2(b). LOG performs better edge detection than the gradient edge detection operators.

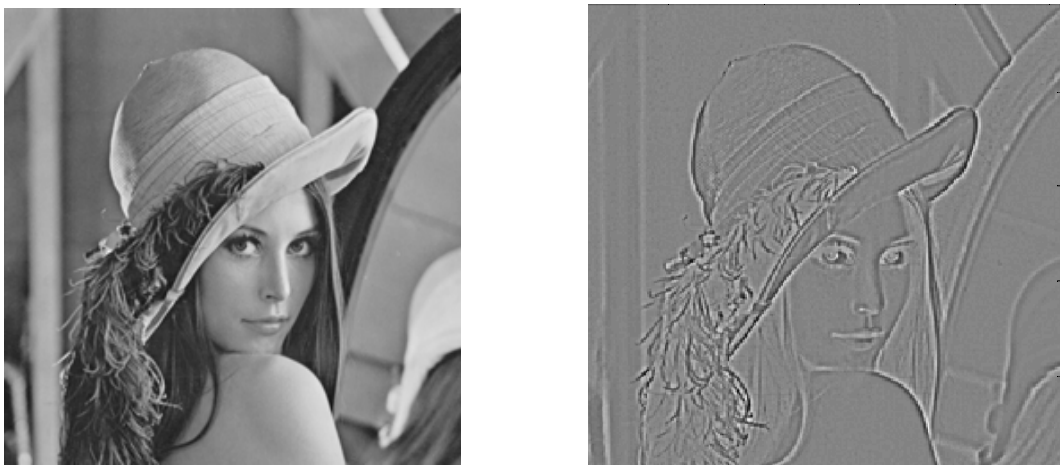

(a) (b)

Figure 5.2: (a) Original noiseless lenna image (b) Laplacian of Gaussian (LOG)

## 5.2 WAVELET EDGE DETECTION OF IMAGE WITHOUT NOISE

Wavelets are used for edge detection to eliminate the difficulties such as the inability of handling large contrast between images and the inability to handle large translations of features. The Haar wavelet transform is the basic and principle wavelet transform which produces essentially edge maps of the vertical, horizontal, and diagonal edges in an image.

Figure 5.3 shows the 1st level wavelet transform using Haar, Daubechies, Coiflets and Biorthogonal wavelets. Further levels of Daubechies wavelets are used for complex problems like images with noise and images of large size where multiple levels of processing is required before doing the edge detection.

The edge detection of lenna image shown in figure 5.4(a) using Haar wavelet is shown in figure 5.4(b). Haar wavelet edge detection produces the vertical, horizontal, and diagonal details, which makes it a better edge detector than the gradient and LOG operators.

Figure 5.4(b) show the edge detection using db2 wavelet. The Haar wavelet edge detection is superior to the db2 edge detection and coif1 edge detection (shown in figure 5.4(d)) for first level decomposition edge detection due to the shape of the wavelet. But once we compute more complex problems with different scales we can observer that the performance of Daublets and coiflets is very impressive compared to Haar wavelet. The edge detection of Bior1.3 shown in figure 5.4(e) is better than Haar due to the basis, which arises from two multiresolution analyses.

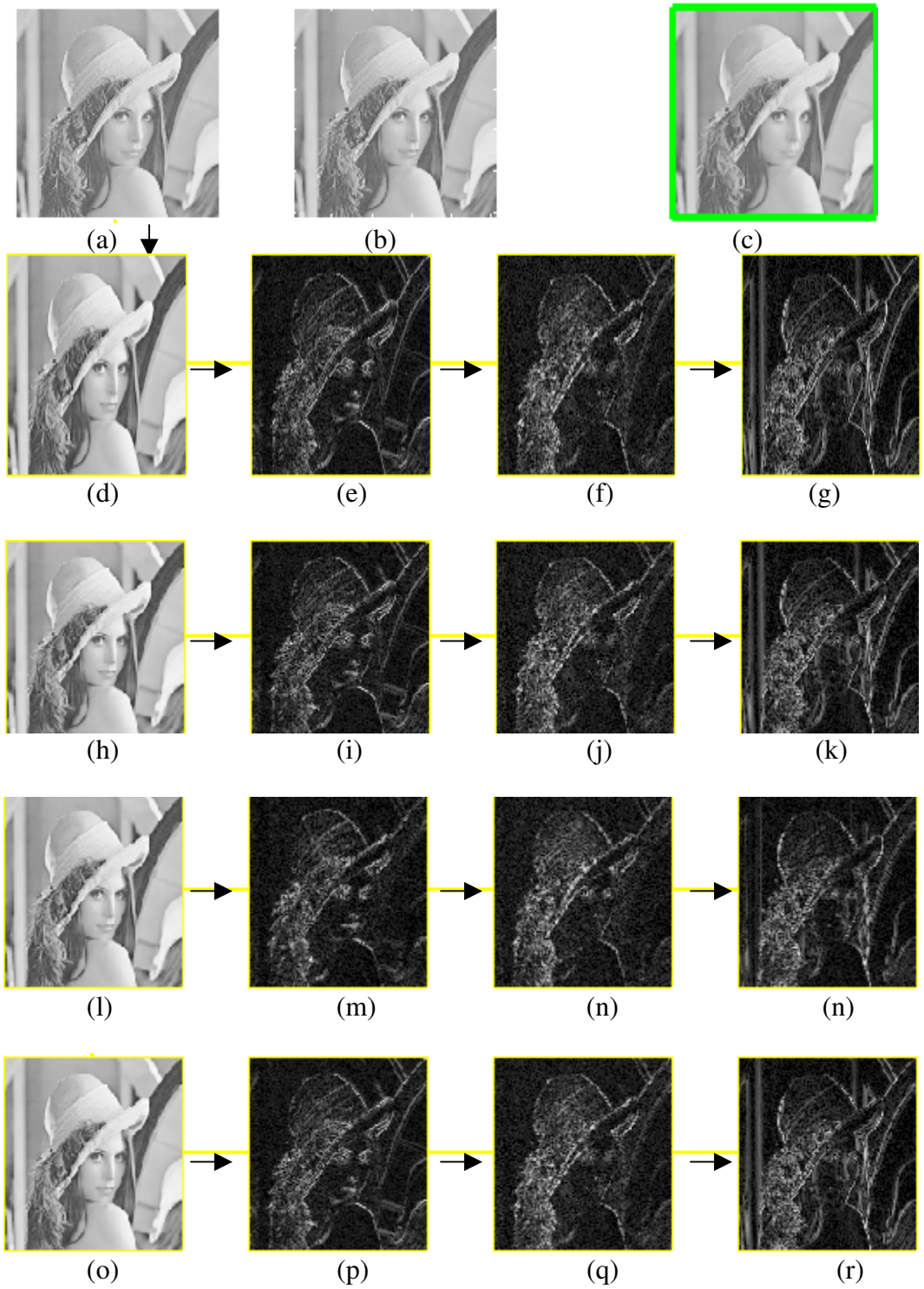


Figure 5.3: DWT of noiseless lenna image using the 4 different wavelets (a) Original lenna image (b) Synthesized image (c) Reconstruction of approximate coefficients using Haar (d) Approximation coefficients image using Haar (e) Horizontal details coefficients image using Haar (f) Vertical details coefficients image using Haar (g) Diagonal details

coefficients image using Haar (h) Approximation coefficients image using db2 (i) Horizontal details coefficients image using Db2
(j) Vertical details coefficients image using Db2 (k) Diagonal details coefficients image using DB2 (l) Approximation coefficients image using coif1 (m) Horizontal details coefficients image using coif1 (n) Vertical details coefficients image using coif1 (o) Diagonal details coefficients image using coif1 (p) Approximation coefficients image using Bior1.3 (q) Horizontal details coefficients image using Bior1.3 (r) Vertical details coefficients image using Bior1.3 (s) Diagonal details coefficients image using Bior1.3

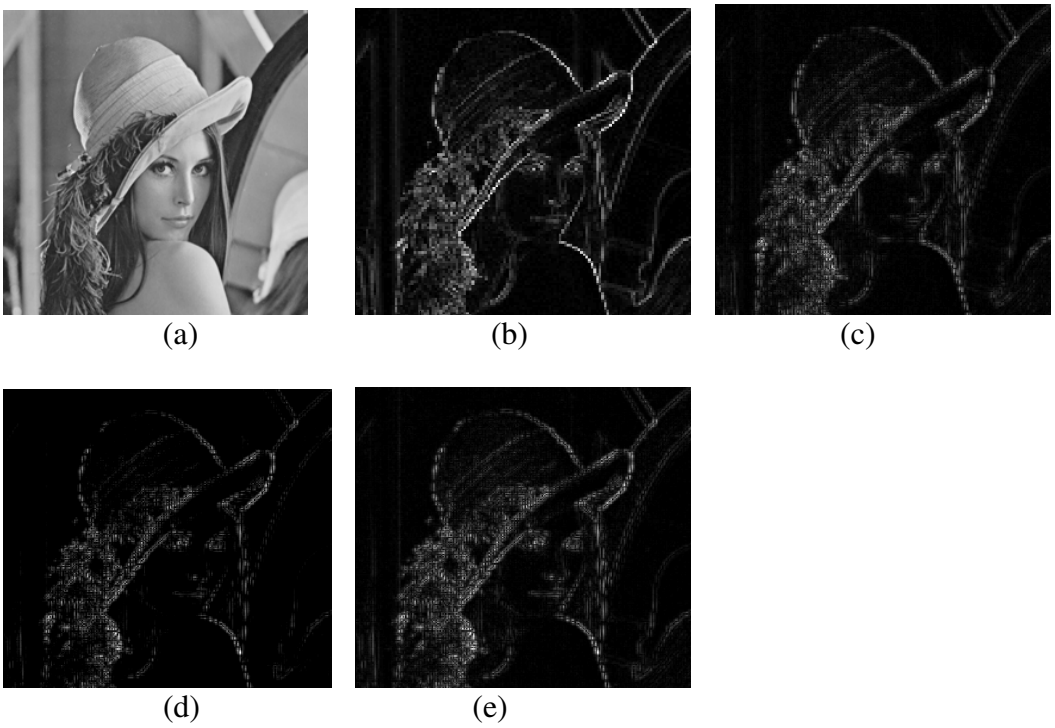


Figure 5.4: Edge detection of noiseless lenna image using wavelets (a) Original lenna image (b) Edge detection using Haar 1st level decomposition (c) Edge detection using Db2 1st level decomposition (d) Edge detection using coif1 1st level decomposition (e) Edge detection using Bior1.3 1st level decomposition

## 5.3 TRADITIONAL EDGE DETECTION OF IMAGE WITH NOISE

Figure 5.5 shows the edge detection on a noisy lenna image. The noise added to the images is salt & pepper with a noise density of 0.02. The salt & pepper noise added image of lenna is shown in figure 5.5(a). Robert operator performs very badly compared to other operator because of the simple mask used. Sobel operator as shown in figure 5.5(c) performs better than Prewitt operator shown in figure 5.5(d) and Frei-Chen operator shown in figure 5.5(e).

The Laplacian of Gaussian edge operator as shown in figure 5.6 picks up a lot of information of the image but also picks up a lot of noise. The edge detection is done without any removal of noise. The LOG operator performs well if some preprocessing of the image like noise removal or thresholding is done. Due to the shape of the LOG operator, it detects a lot of noise. The LOG operator smoothens the image thereby blurring the image, which makes it a bad operator if preprocessing is not performed.

(a)

(b)

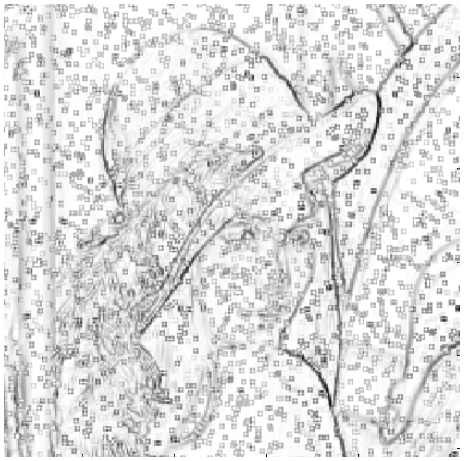

(c)

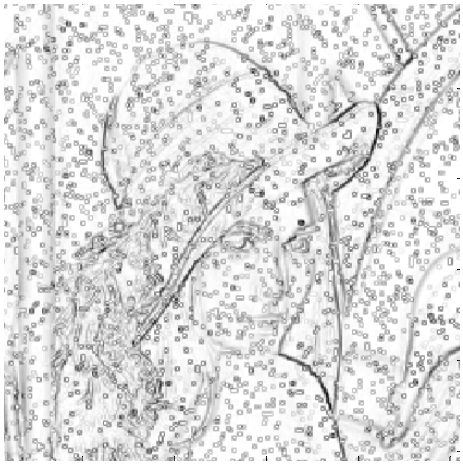

(d)

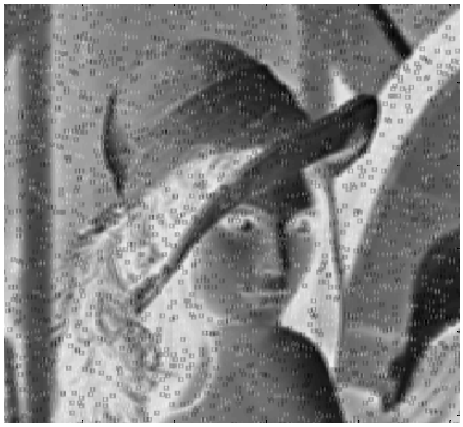

(e)

Figure 5.5: Edge detection of noisy lenna image using Gradient edge detectors (a) Original lenna image with salt & pepper noise (b) Robert edge detection (c) Prewitt edge detection (d) Sobel edge detection (e) Frei-chen edge detection

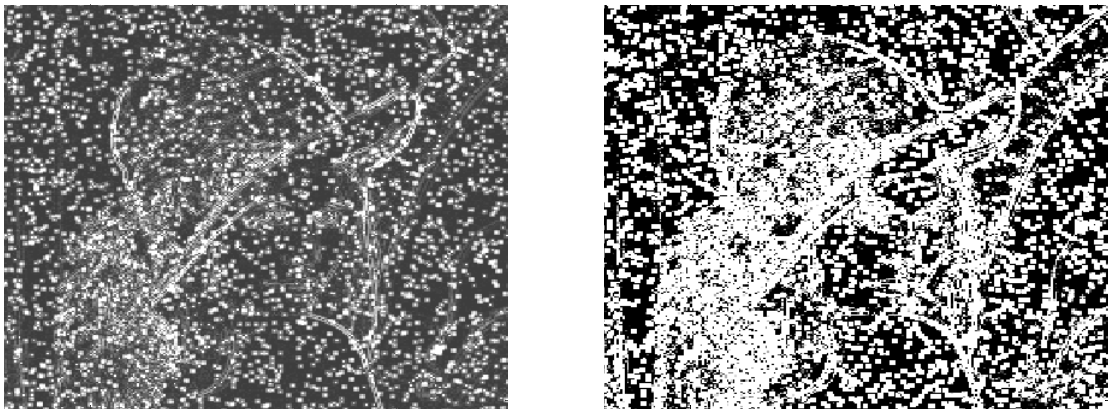

(a) (b)

Figure 5.6: Edge detection of noisy lenna image LOG edge detectors (a) edge detection using LOG with a minimal processing (b) edge detection-using LOG without processing.

## 5.4 WAVELET EDGE DETECTION OF IMAGE WITH NOISE

We perform edge detection using all the 4-wavelet families without using the different level in each of the wavelet family. The edge detection using multistage is discussed in the next section. The first level decomposition of noisy lenna image using Haar, Daubechies, Coifman and Biorthogonal wavelets is shown in figure 5.7.

The results of edge detection performed on noisy lenna image are shown in figure 5.8. The edge detection is done on the first decomposition level only. Biorthogonal wavelet performs the best edge detection compared to the other wavelets.

Biorthogonal wavelet suppresses a lot of noise in one level of decomposition only. Daubechies wavelets perform well compared to coiflets. Haar wavelet also suppresses a decent amount of impurities thereby giving good result.

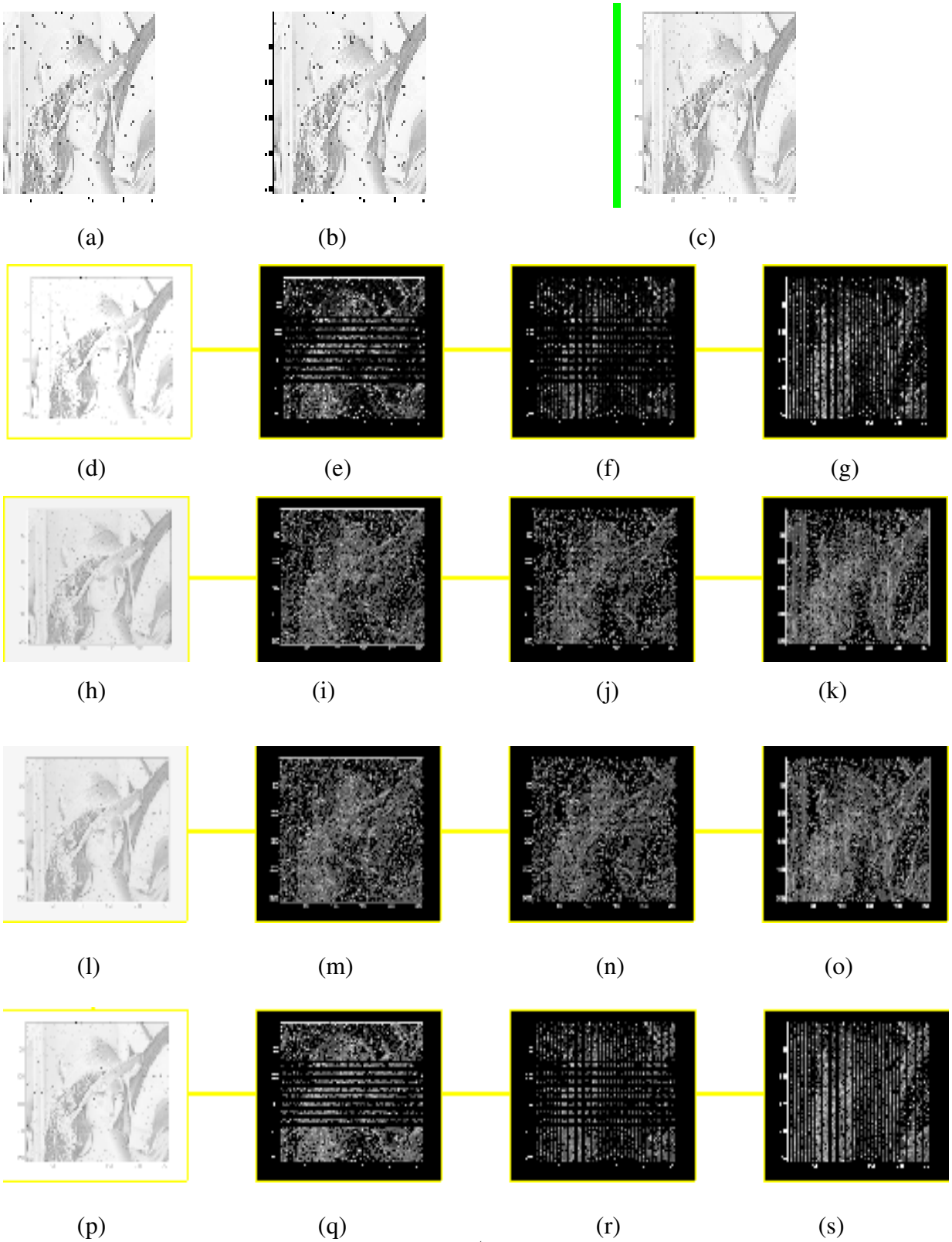


Figure 5.7: DWT of noisy lenna image at 1st level using all 4 different wavelets (a) Original noisy lenna image (b) Synthesized image (c) Reconstruction of approximate coefficients using Haar (d) Approximation coefficients image using Haar (e) Horizontal

details coefficients image using Haar (f) Vertical details coefficients image using Haar (g) Diagonal details coefficients image using Haar (h) Approximation coefficients image using db2 (i) Horizontal details coefficients image using Db2
(j) Vertical details coefficients image using Db2 (k) Diagonal details coefficients image using DB2 (l) Approximation coefficients image using coif1 (m) Horizontal details coefficients image using coif1 (n) Vertical details coefficients image using coif1 (o) Diagonal details coefficients image using coif1 (p) Approximation coefficients image using Bior1.3 (q) Horizontal details coefficients image using Bior1.3 (r) Vertical details coefficients image using Bior1.3 (s) Diagonal details coefficients image using Bior1.3

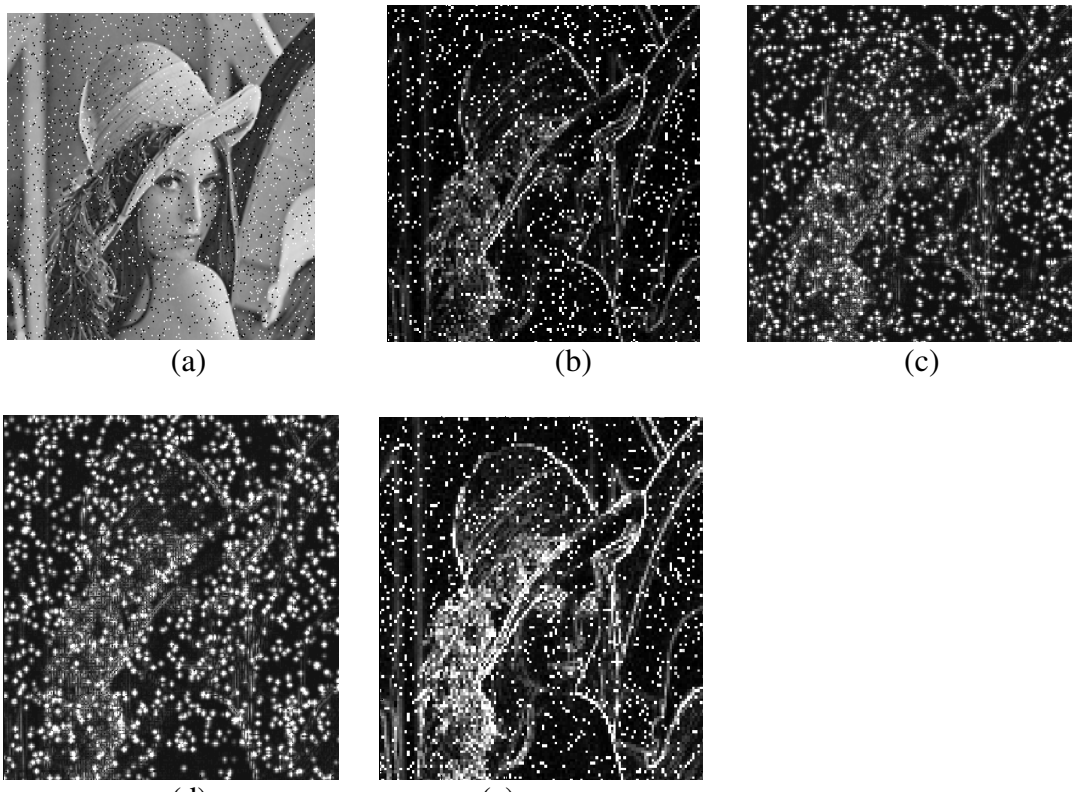

(a) (b) (c)

(d) (e)

Figure 5.8: Edge detection of noisy lenna image using 1st level DWT (a) Original lenna image (b) Edge detection using Haar (c) Edge detection using Db2 (d) Edge detection using coif1 (e) Edge detection using Bior1.3

## 5.5 MULTISCALE WAVELET EDGE DETECTION

Mallat proved that the 1D implementation of the Mallat-Zhong DWT has perfect reconstruction and is a stable representation i.e. the wavelet coefficients decay appropriately [19]. However, the 2D Mallat-Zhong DWT does not have perfect reconstruction, because the diagonal detail coefficients are not calculated. It is sufficient to compute the horizontal and vertical wavelet coefficients for edge detection. Thus computation can be sped-up by ignoring the diagonal coefficients at the cost of perfect reconstruction. However, the 2D transform is also stable and even without perfect reconstruction a reconstructed image is visually indistinguishable from the original image.

### 5.5.1 EDGE DETECTION AT LEVEL 2

The edge detection of lenna image using the Haar wavelet at the second level is shown in figure 5.9. Haar wavelet works very well at the first level but it fails when multiscale edge detection is applied due to the simplicity of the wavelet. Its inability to remove noise when the image is further decomposed is shown in figure 5.9(h).

Compared to the Haar wavelet edge detection Daubechies wavelet suppresses a lot of noise as shown in figure 5.10, and the edge detection thereby is better than that of Haar edge detection. As we increase the scale of Daubechies wavelet the performance of edge detection is improved unlike Haar.

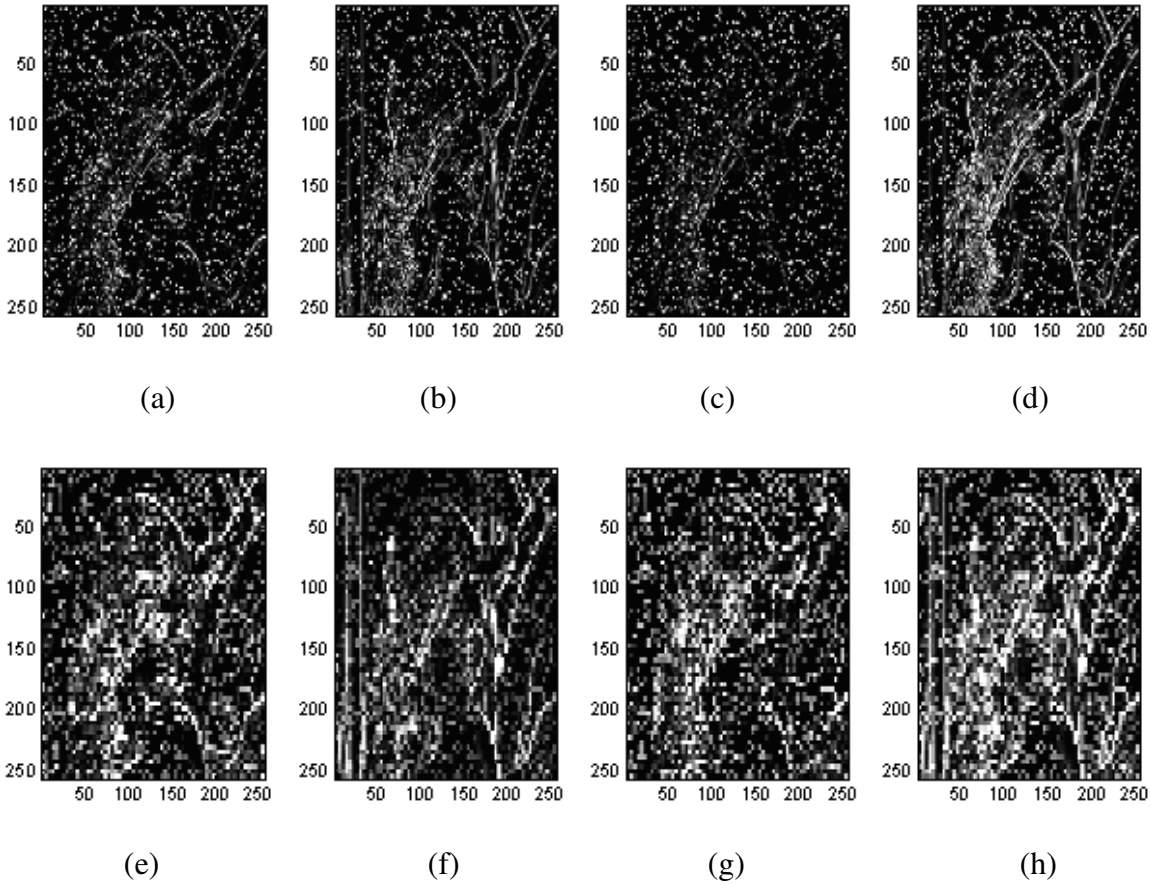


Figure 5.9: Edge detection of lenna image using Haar wavelet at 1st and 2nd levels (a) Horizontal detail coefficients of Haar 1st level (b) Vertical detail coefficients of Haar 1st level (c) Diagonal detail coefficients of Haar 1st level (d) Edge detection using Haar 1st level (e) Horizontal detail coefficients of Haar 2nd level (f) Vertical detail coefficients of Haar 2nd level (g) Diagonal detail coefficients of Haar 2nd level (h) Edge detection using Haar 2nd level

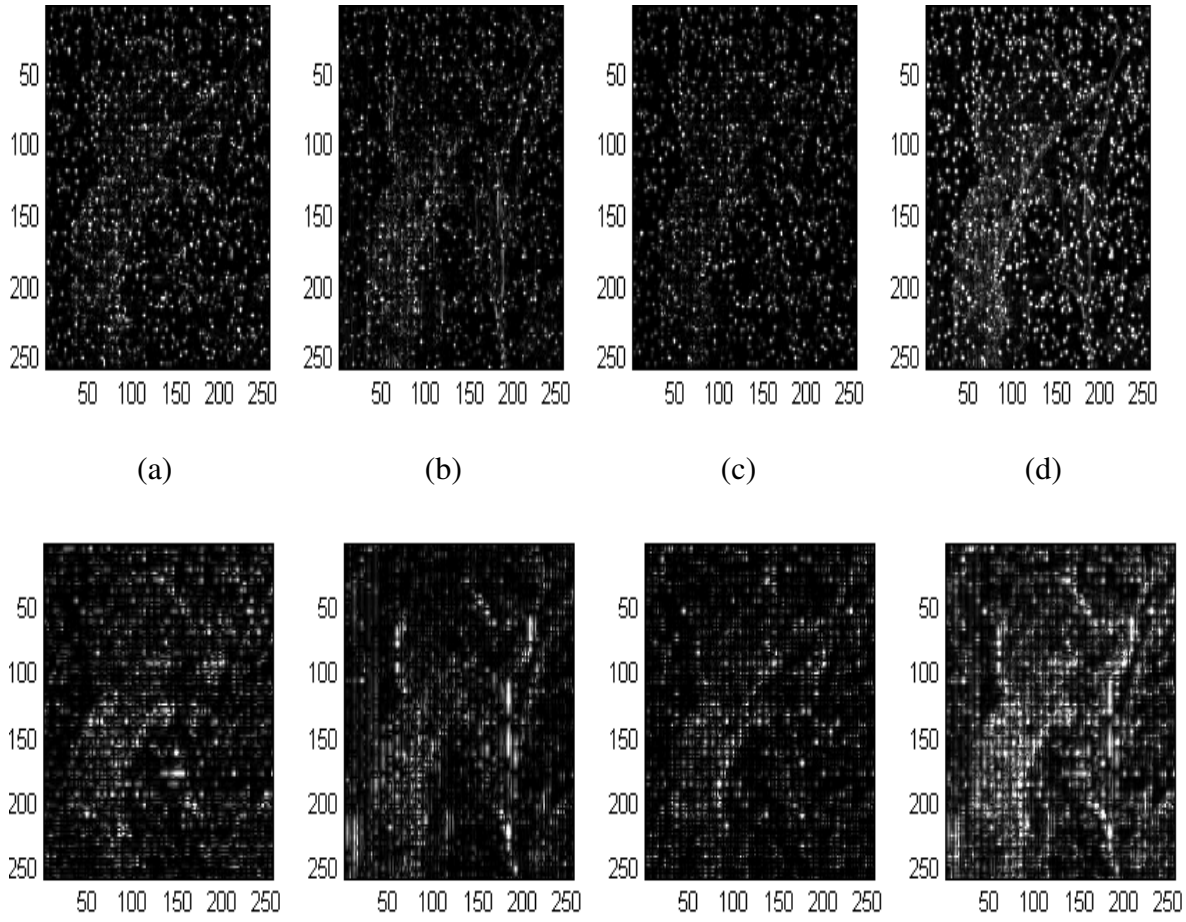


Figure 5.10: Edge detection of lenna image using db2 wavelet at 1st and 2nd levels (a) Horizontal detail coefficients of db2 1st level (b) Vertical detail coefficients of db2 1st level (c) Diagonal detail coefficients of db2 1st level (d) Edge detection using db2 1st level (e) Horizontal detail coefficients of db2 2nd level (f) Vertical detail coefficients of db2 2nd level (g) Diagonal detail coefficients of db2 2nd level (h) Edge detection using db2 2nd level

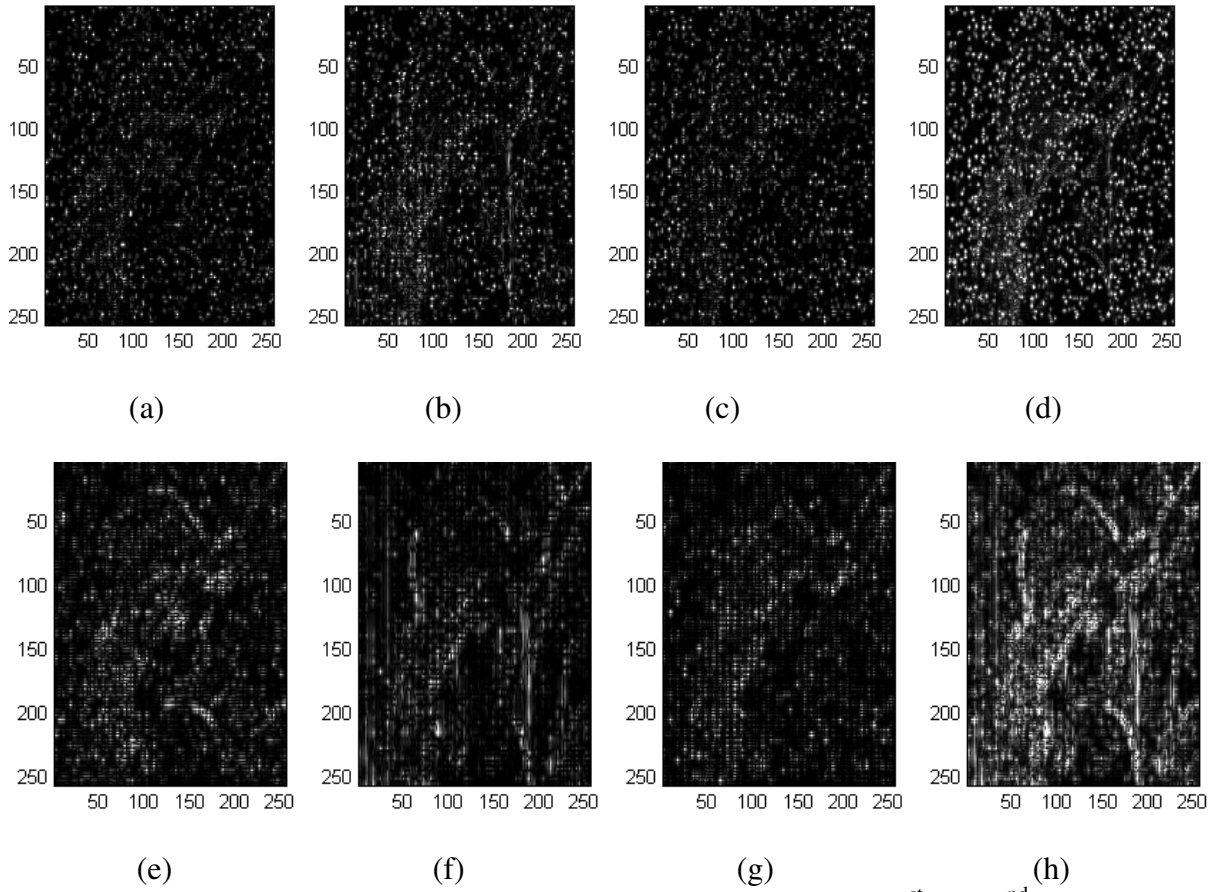


Figure 5.11: Edge detection of lenna image using coif1 wavelet at 1st and 2nd levels (a) Horizontal detail coefficients of coif1 1st level (b) Vertical detail coefficients of coif1 1st level (c) Diagonal detail coefficients of coif1 1st level (d) Edge detection using coif1 1st level (e) Horizontal detail coefficients of coif1 2nd level (f) Vertical detail coefficients of coif1 2nd level (g) Diagonal detail coefficients of coif1 2nd level (h) Edge detection using coif1 2nd level

Coiflets pick up more details (as shown in figure 5.11(h)) than both db2 and Haar. The edge detection compared to its first level is much better. It reduces a large amount of noise by just going one level down. Biorthogonal wavelets also perform well as we increase the scale. These wavelets also reduce the noise and enhance the edge in an image as shown in figure 5.12.

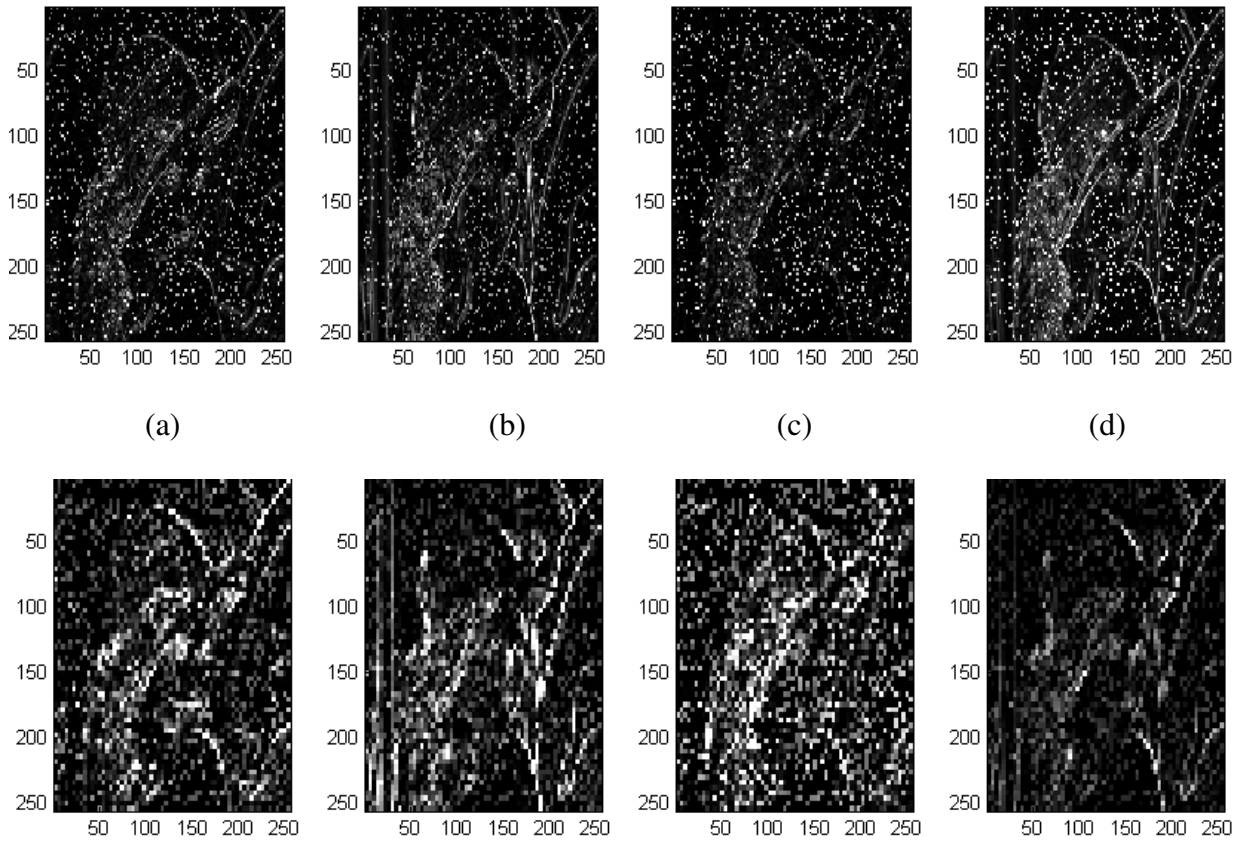


Figure 5.12: Edge detection of lenna image using Bior1.3 wavelet at 1st and 2nd levels (a) Horizontal detail coefficients of Bior1.3 1st level (b) Vertical detail coefficients of Bior1.3 1st level (c) Diagonal detail coefficients of Bior1.3 1st level (d) Edge detection using Bior1.3 1st level (e) Horizontal detail coefficients of Bior1.3 2nd level (f) Vertical detail coefficients of Bior1.3 2nd level (g) Diagonal detail coefficients of Bior1.3 2nd level (h) Edge detection using Bior1.3 2nd level

### 5.5.2 EDGE DETECTION AT LEVEL 3

Daubechies wavelet Coifman wavelet Biorthogonal wavelet

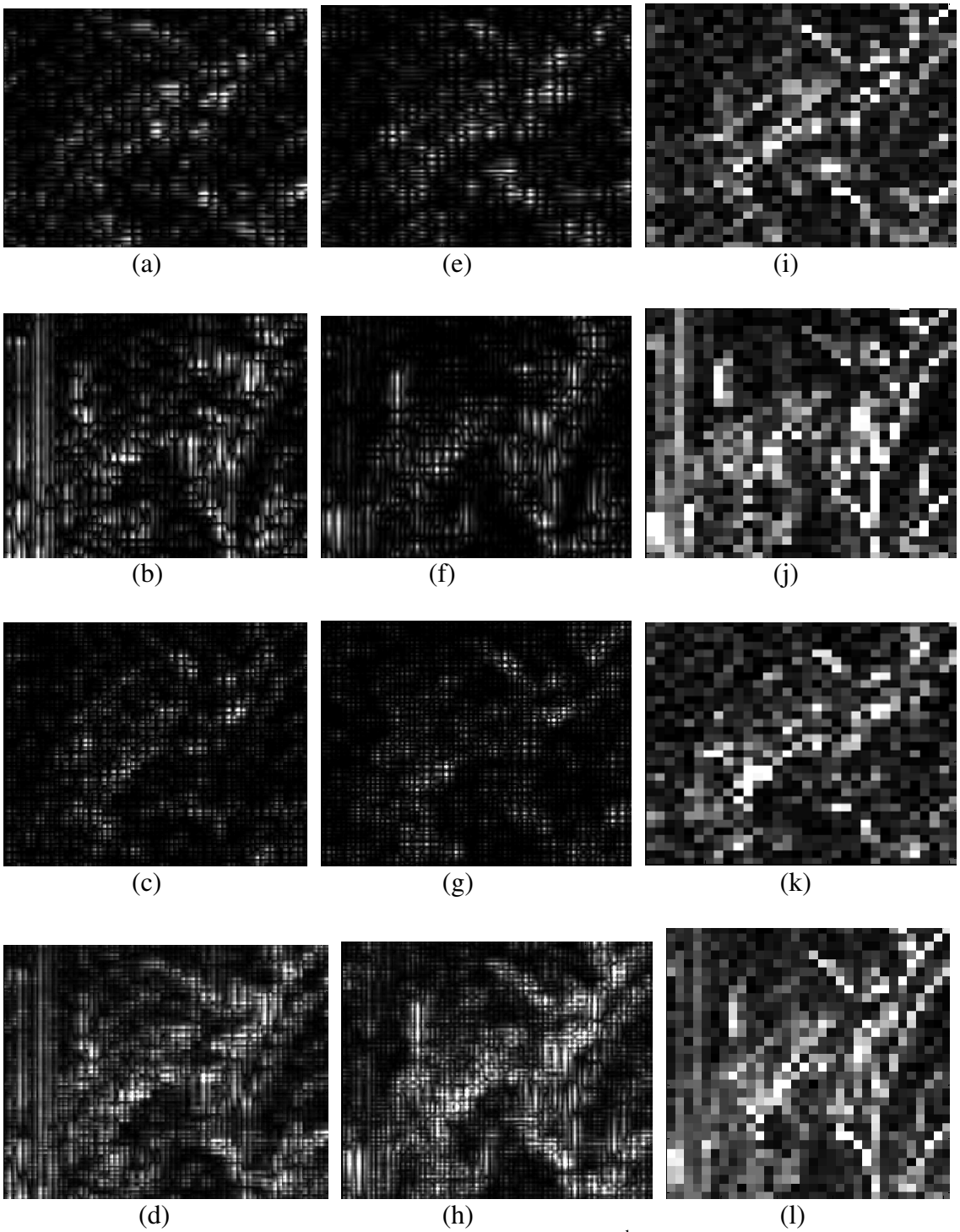

(a) (e) (i)

(b) (f) (j)

(c) (g) (k)

(d) (h) (l)

Figure 5.13: Wavelet analysis on noisy lenna image at 3rd level for db2, coif1 and bior1.3 (a) Horizontal detail coefficients of db2 3rd level (b) Vertical detail coefficients of db2 3rd level (c) Diagonal detail coefficients of db2 3rd level (d) Edge detection using db2 3rd

level (e) Horizontal detail coefficients of coif1 3rd level (f) Vertical detail coefficients of coif1 3rd level (g) Diagonal detail coefficients of coif1 3rd level (h) Edge detection using coif1 3rd level (i) Horizontal detail coefficients of Bior1.3 3rd level (j) Vertical detail coefficients of Bior1.3 3rd level (k) Diagonal detail coefficients of Bior1.3 3rd level (l) Edge detection using Bior1.3 3rd level

The 3rd level edge detection of noisy lenna image is shown in figure 5.13. Both coiflets and daublets perform a good job in removing the noise and enhancing the edges. When it comes to the biorthogonal wavelets, this also removes a great amount of noise but due to the low pixel count of the original image, the detail coefficients are blurred.

## 5.6 QUANTITATIVE ANALYSIS OF EDGE DETECTORS

Figure 5.14 shows the graph of the performance of tradition edge operators on noisy images. The graph is plotted with signal to noise ratio against the noise density of the salt & pepper noise. Frei-Chen performs extremely well with respect to the signal to noise ratio. The LOG operator also performs well compared to the other operators.

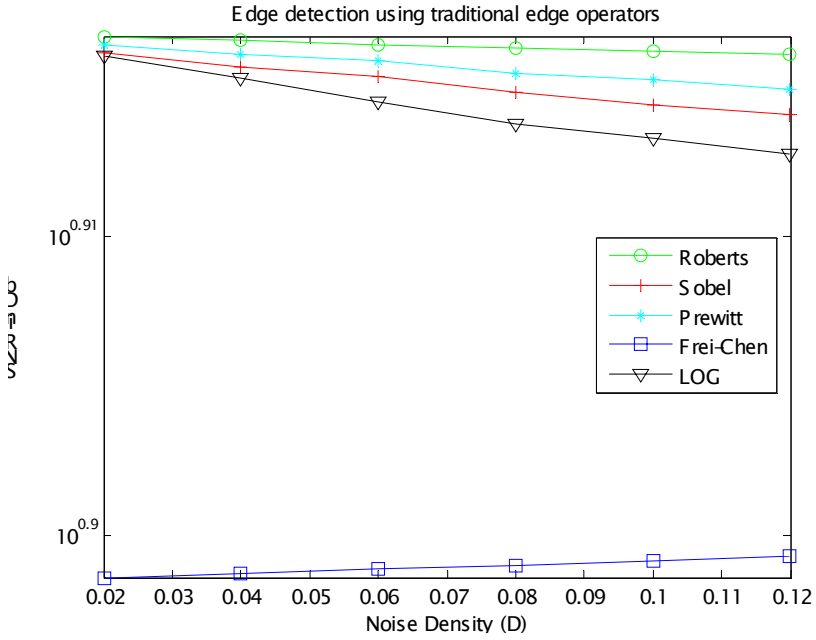


Figure 5.14: Graphical performance of Edge detection using traditional edge operators

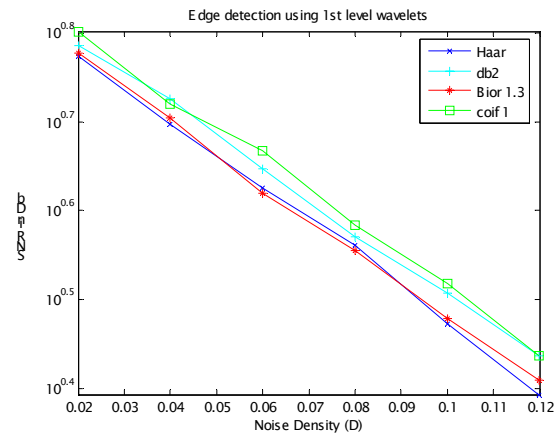


(a)

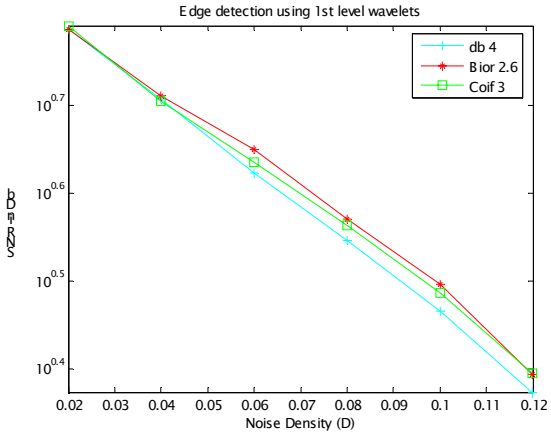


(b)

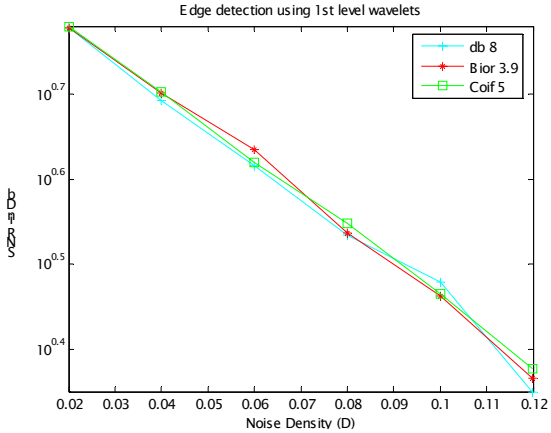


(c)

Figure 5.15: Graphical performance of 1st level wavelet edge detection

Figure 5.15 shows the graph of the performance of 1st level wavelet edge detectors on noisy images. Figures 5.15(b) shows the edge detection performance using db4, Bior 2.6 and Coif 3. Similarly figures 5.15(c) shows the edge detection performance using db8, Bior 3.9 and Coif 5.Biorthogonal wavelets perform well in comparision with other wavelets.

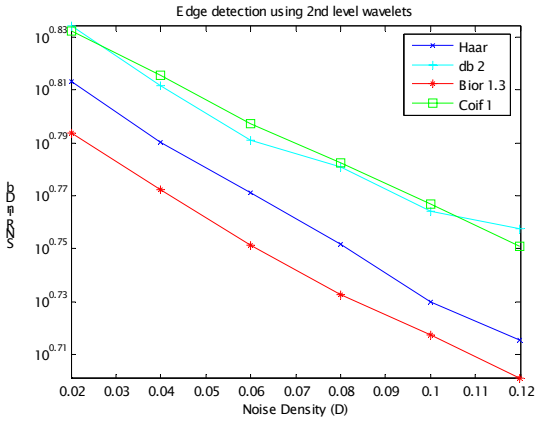


(a)

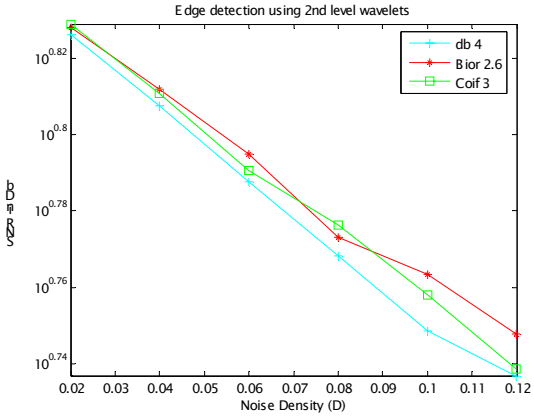


(b)

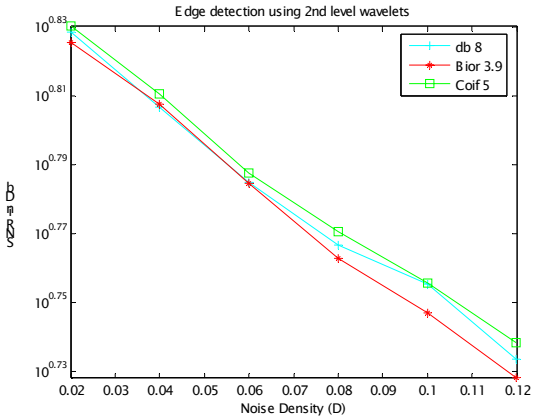


(c)

Figure 5.16: Graphical performance of 2nd level wavelet edge detection

Figure 5.16 shows the graph of the performance of 2nd level wavelet edge detectors on noisy images. Coiflets and Daublets perform well at the 2nd level. They have a higher SNR. But when the edge detection is performed with higher wavelets of biothogonal wavelets like Bior 2.6 or Bior 3.9, they have a better edge detection property.

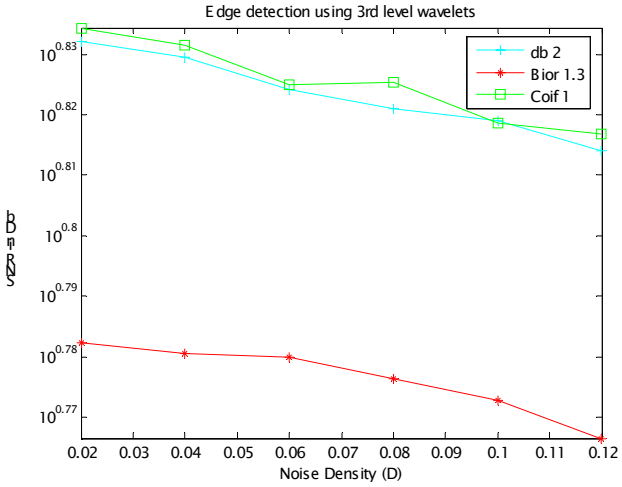


(a)

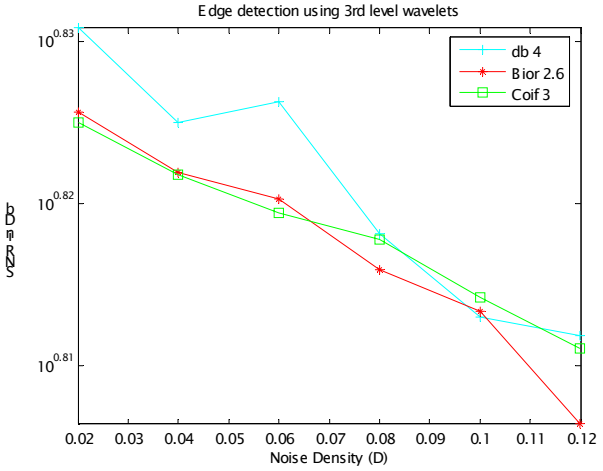


(b)

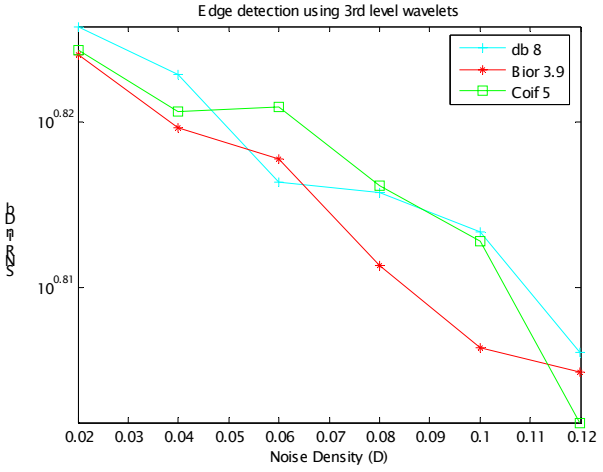


(c)

Figure 5.17: Graphical performance of 3rd level wavelet edge detection

Figure 5.16 shows the graph of the performance of 2nd level wavelet edge detectors on noisy images. At the 3rd level the SNR of both the coiflets and daublets is better but biorthogonal wavelets reduces more noise.

# CHAPTER 6

## CONCLUSION AND FUTHER RESEARCH

Edge detection is a very important problem in image processing. We studied the problems faced by traditional edge detectors with noisy images. We proved that wavelets are more functional and better edge detectors both theoretically and experimentally. We briefly review the key contributions of this thesis below.

In this thesis we have developed an algorithm for the multiscale wavelet edge detection. The comparison of wavelets and traditional edge detection techniques on images in noisy environment is performed. The different methods of multiscale wavelet edge detection are studied. A database of images in noisy environment is subjected to edge detection using wavelets and the results are tabulated.

In Chapter 1, we discussed about edge detection and the influence of noise in an image on edge detection. We also discussed the evolution of wavelets from Fourier transform.

In Chapter 2, we established the mathematical theory for both the wavelet transforms and the construction of wavelets. We also discussed the mathematical aspect of wavelet decomposition and reconstruction.

In Chapter 3, we dealt with both the gradient and Laplacian edge detectors and the reason for there failure with noisy images. We performed a behavioral study of traditional edge detectors.

In Chapter 4, we develop an algorithm for discrete wavelet transform edge detection. We also discuss the mathematical theory of four different wavelet families. We also discuss the development complexities of each of the four different wavelet families.

In Chapter 5, we develop an algorithm for multiscale edge detection with the four different wavelet families. The results are tabulated and a comparison between the traditional and wavelet based edge detectors are computed. We prove it experimentally that discrete wavelet transform edge detection is superior to traditional edge detection. The comparison between the four different wavelets is also performed and an optimal wavelet for edge detection is evaluated.

Although the wavelet transform is a good decorrelator for images, the wavelet coefficients of natural images exhibit strong dependencies both across scales and between neighbor coefficients within a subband, especially around image edges. This gave rise to several successful joint statistical models in the wavelet domain as well as improved image compression schemes. The major drawback for wavelets in two-dimensions is their limited ability in capturing directional information.

We propose some problems related the edge detection using discrete wavelet transform, which may worth future research works.

1.) Edges exhibit discontinuities across curves in real world images, which contain a lot of noise. Curvelet are a temporary solution for this problem, but the complexity of curvelets is extremely high. A faster and simpler wavelet analysis needs to be studied and developed.
2.) Inspired from curvelets, Inspired by curvelets, Do and Vetterli developed the contourlet transform based on an efficient two-dimensional multiscale and directional filter bank that can deal effectively with images having smooth contours. Edge detection and comparison of real world noisy images using contourlet transform would be a good research topic.

## REFERENCES


[1] Rafael C. Gonzales, Richard E. Woods, Digital Image Processing, second edition, Prentice Hall, 2002

[2] Raghuveer M. Rao, Ajit S. Bopardikar, Wavelet transforms: Introduction to theory and applications, Pearson Education, Inc., 1998

[3] Y.T. Chen, Wavelet Basics, Kluwer Academic Publishers, 1995

[4] Yves Nievergelt, Wavelets Made Easy, Birkhauser Boston, 1999

[5] Gilbert Strang, Truong Nguyen, Wavelets and Filter banks, Wellesley-Cambridge Press, 1997

[6] David F. Walnut, An Introduction to Wavelet Analysis, Birkhauser Boston, 2002

[7] Albert Boggess, Francis J. Narcowich, A First Course in Wavelets with Fourier Analysis, Prentice Hall, 2001

[8] Barbara Burke Hubbard, The World According to Wavelets: The story of a mathematical techniques in the Making, second edition, A.K. Peters, Ltd., 1998

[9] Jaideva C. Goswami, Andrew K. Chan, Fundamentals of Wavelets, John Wiley & Sons, Inc., 1999

[10] Michel Misiti, Yves Misiti, George Oppenheim, Jean-Michel Poggi, Wavelet Toolbox: For Use with Matlab, The Mathworks, Inc., 1996

[11] Grant V. Welland, Beyond Wavelets, Academic Press, 2003

[12] Edward Aboufadel and Steven Schlicker, Discovering Wavelets, John Wiley & Sons, Inc., 1999

[13] James S. Walker, A Primer on Wavelets and their Scientific Applications, CRC Press LLC, 1999

[14] Fritz Keinert, Wavelets and Multiwavelets, CRC Press LLC, 2004

[15] Albert Cohen, Numerical Analysis Of Wavelet Methods, Elsevier Science B.V, 2003

[16] Ola Bratteli, Palle Jorgensen, Wavelets through a Looking glass: The World of the Spectrum, Birkhauser Boston, 2002

[17] S. Mallat, S. Zhong, "Characterization of Signals from Multiscale Edges," IEEE Transactions on Pattern Analysis and Machine Intelligence, Vol. 14, No.7, July 1992

[18] S. Mallat, A Wavelet Tour of Signal Processing 2ed, Academic Press: 1999

[19] S. Mallat, W. L. Hwang, "Singularity Detection and Processing with Wavelets," IEEE Transactions of Information Theory, Vol. 38, No.2, March 1992

[20] Fei Shen, Han Wang, "A local edge detector used for finding corners", April 1997

[21] Barlaud, M.; Gaidon, T.; Mathieu, P.; Feauveau, J.C., "Edge detection using recursive biorthogonal wavelet transform ", Acoustics, Speech, and Signal Processing, 1991. ICASSP-91., 1991 International Conference on 14-17 April 1991 Page(s):2553 - 2556 vol.4

[22] Rao, R.M., "Biorthogonal generalization of Meyer wavelets", Signals, Systems & Computers, 1997. Conference Record of the Thirty-First Asilomar Conference on Volume 2, 2-5 Nov. 1997 Page(s):1240 - 1243 vol.2

[23] Young-Hyun Baek, Oh-Sung Byun, Sung-Rung Moon, "Image edge detection using adaptive morphology Meyer wavelet", Neural Networks, 2003. Proceedings of the International Joint Conference on Volume 2, 20-24 July 2003 Page(s):1219 - 1222 vol.2

[24] Aldroubi, A., Abry, P., Unser, M., "Construction of biorthogonal wavelets starting from any two multiresolutions", Signal Processing, IEEE Transactions on Acoustics, Speech, and Signal Processing, IEEE Transactions on Volume 46, Issue 4, April 1998 Page(s):1130 – 1133

[25] Dong Wei, Bovik, A.C., Evans, B.L, "Generalized coiflets: a new family of orthonormal wavelets", Signals, Systems & Computers, 1997. Conference Record of the Thirty-First Asilomar Conference on Volume 2, 2-5 Nov. 1997 Page(s):1259 - 1263 vol.2

[26] Beltran, J.R., Garcia-Lucia, J., Navarro, J., **"**Edge detection and classification using Mallat's wavelet", Image Processing, 1994. Proceedings. ICIP-94., IEEE International Conference Volume 1, 13-16 Nov. 1994 Page(s):293 - 297 vol.1

[27] Chabert, M., Tourneret, J.-Y., Mesnager, G., "Edge detection in speckled SAR images using the continuous wavelet transform", Geoscience and Remote Sensing Symposium, 1996. IGARSS '96. 'Remote Sensing for a Sustainable Future.', International Volume 3, 27-31 May 1996 Page(s):1842 - 1844 vol.3

[28] Manjunath B.S., “A unified approach to boundary perception: edges, textures and illusory contours”, IEEE transactions on Neural networks, vol. 4, no. 1, January 1993

[29] Karrakchou, M.; Li, W., “Optimal ramp edge detection by orthogonal wavelet transform”, Circuits and Systems, 1992. ISCAS '92. Proceedings, 1992 IEEE International Symposium on Volume 2, 3-6 May 1992 Page(s):967 - 970 vol.2

[30] Wang X.H., Robert S.H. Istepanian, Yong Hua Song, “Application of wavelet modulus maxima in microarray spots recognition”, IEEE transactions on Nanobioscience, vol.2, no.4, December 2003

[31] Lee, J.S., Sun, Y.N., Chen, C.H, “Wavelet transform for corner detection”, Systems Engineering, 1992, IEEE International Conference on 17-19 Sept. 1992 Page(s):596 – 599

[32] Akujuobi, C.M., “The effects of different wavelets on image reconstruction”, Southeastcon '96. 'Bringing Together Education, Science and Technology’, Proceedings of the IEEE 11-14 April 1996 Page(s):293 – 296

[33] Rifaat, R., Kinsner, W., “Experiments with wavelet and other edge detection techniques”, WESCANEX 97: Communications, Power and Computing. Conference Proceedings, IEEE 22-23 May 1997 Page(s):322 – 326

[34] Jong-Chih Chien, Li, C.C., “Wavelet-based line detection in gray-scale images”, Systems, Man, and Cybernetics, 1997. 'Computational Cybernetics and Simulation’, 1997 IEEE International Conference on Volume 4, 12-15 Oct. 1997 Page(s):3670 - 3673 vol.4

[35] Siddique, J.I., Barner, K.E., “Wavelet-based multiresolution edge detection utilizing gray level edge maps”, Image Processing, 1998. ICIP 98. Proceedings. 1998 International Conference on Volume 2, 4-7 Oct. 1998 Page(s):550 - 554 vol.2

[36] Zeng Luan, Xiong Wei, Xie Jian Wei, “Edge detection of image based on the B-wavelet transform”, Signal Processing Proceedings, 1998. ICSP '98. 1998 Fourth International Conference on Volume 2, 12-16 Oct. 1998 Page(s):998 - 1001 vol.2

[37] Berkner, K., Wells, R.O., Jr., “A new hierarchical scheme for approximating the continuous wavelet transform with applications to edge detection”, Signal Processing Letters, IEEE Volume 6, Issue 8, Aug. 1999 Page(s):193 – 195

[38] Candes, E, “The curvelet transform for image denoising”, Image Processing, 2001. Proceedings. 2001 International Conference on Volume 1, 7-10 Oct. 2001 Page(s):7 vol.1

[39] Lei Zhang, Bao, P., “A wavelet-based edge detection method by scale

multiplication", Pattern Recognition, 2002. Proceedings. 16th International Conference on Volume 3, 11-15 Aug. 2002 Page(s):501 - 504 vol.3

[40] Kim, H.J., Kim, W., Li, C.C., "A performance study of two wavelet-based edge detectors", Pattern Recognition, 1992. Vol.III. Conference C: Image, Speech and Signal Analysis, Proceedings, 11th IAPR International Conference on 30 Aug.-3 Sept. 1992 Page(s):302 – 306

[41] Laligant, O., Truchete, F., Miteran, J., "Edge detection by multiscale merging", Time-Frequency and Time-Scale Analysis, 1994., Proceedings of the IEEE-SP International Symposium on 25-28 Oct. 1994 Page(s):237 – 240

[42] I. Daubechies, "Ten Lectures on Wavelets," CBMS Regional Conference Series in Applied Mathematics no. 61, SIAM, 1992.

[43] M. Frazier, B. Jawerth, G.L. Weiss, "Littlewood-Paley Theory and the Study of Function Spaces," CBMS Regional Conference Series # 79, American Mathematical Society, 1991.

[44] Marr, D. and Vaina, L., "Representation and recognition of the movements of shapes", Proceedings of the Royal Society of London B, 214:501-524, 1982

[45] Ronald R. Coifman, Guido Weiss**,** "Maximal Functions and Hp Spaces Defined by Ergodic Transformations", National Academy of Sciences, PNAS, vol. 70, no. 6, 1761-1763 June 1, 1973

[46] Jon Harald Kaspersen, Thomas Lango, Frank Lindseth, "Wavelet-based edge detection in ultrasound images", Ultrasound in Med. & Biol., Vol. 27, No. 1, pp. 89–99, 2001

[47] Grossman, A. and Morlet J., "Decomposition of Hardy functions into Square Integrable Wavelets of Constant Shape", SIAM J. Math Anal. 15, p. 723, 1984

[48] Yves Meyer, "Wavelets and operators", Cambridge Studies in Advanced Math., vol. 37, Cambridge Univ. Press, Cambridge, 1992

[49] C. K. Chui and J. Z. Wang, "On compactly supported wavelets and a duality principle", Trans. Amer. Math. Soc. 330 (1992), 903{916.

[50] F. Bergholm, "Edge focusing", In Proc. International Conference on Pattern Recognition, pages 597–600, 1986.

[51] J. Canny, "A computational approach to edge detection", IEEE Trans. on Pattern Analysis and Machine Intelligence, 8(6):679–698, 1986

## BIOGRAPHICAL SKETCH

Venkata R. Chaganti was born in Visakhapatnam, India on June 22nd, 1979. After finishing High School at Timpany School in Visakhapatnam he went to Andhra University, Visakhapatnam to obtain his Bachelors in Electronics and Communications Engineering. In the Fall of 2001, he enrolled in the Masters program in Electrical and Computer Engineering at the Florida State University.

He was awarded the graduate assistantship through out his course of study at the Florida State University. He was the captain for the Florida State University Cricket team. For his M.S. thesis he began working for Dr. Simon Y. Foo on Wavelets for signal and image processing. Venkata is currently taking a break from academics and plans to travel around the USA.